Université de Lille

(More)
Introduction to multi-anvil techniques at synchrotrons

N. Hilairet

LVP for high-pressure experiments

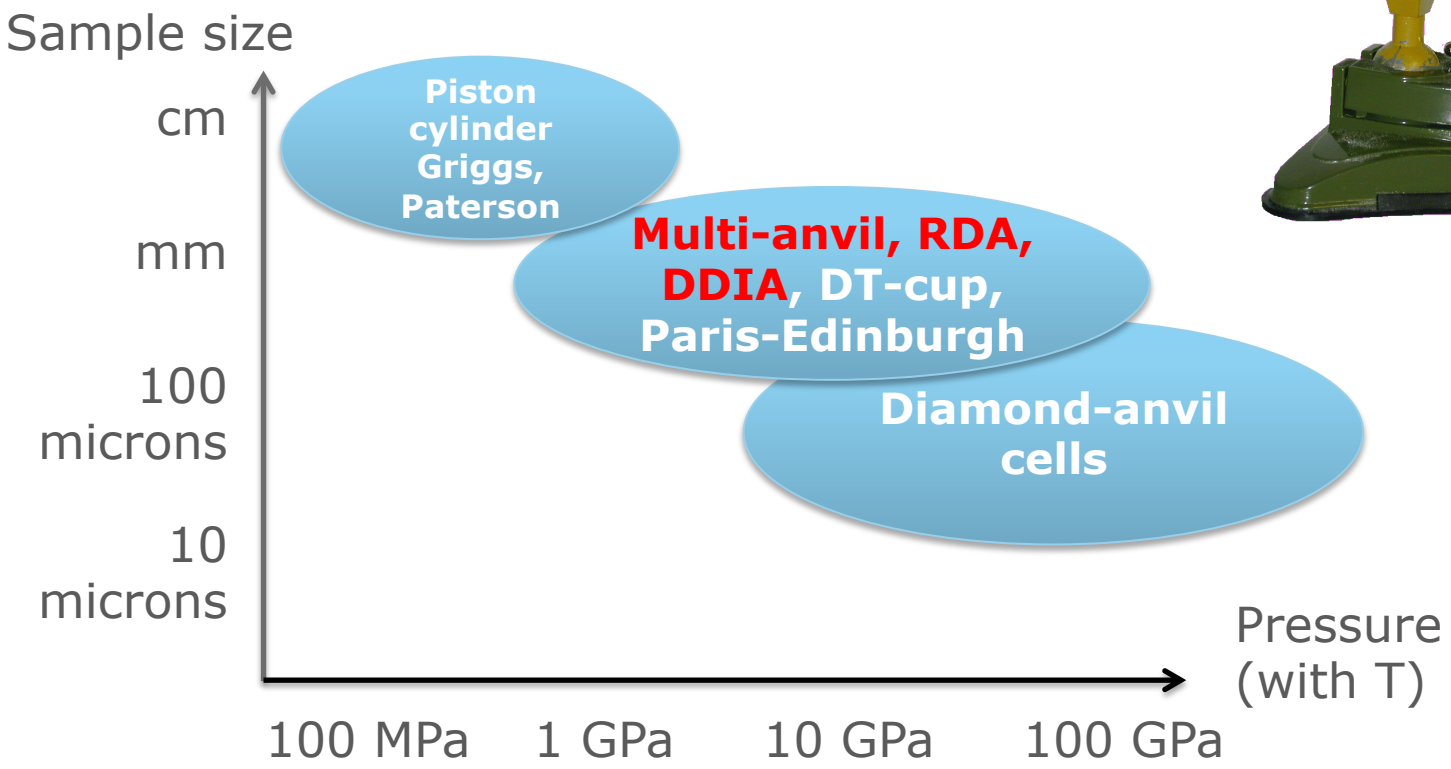

More on LVP and synchrotron adaptations

Multi-anvils at synchrotron beamlines (maybe non exhaustive)

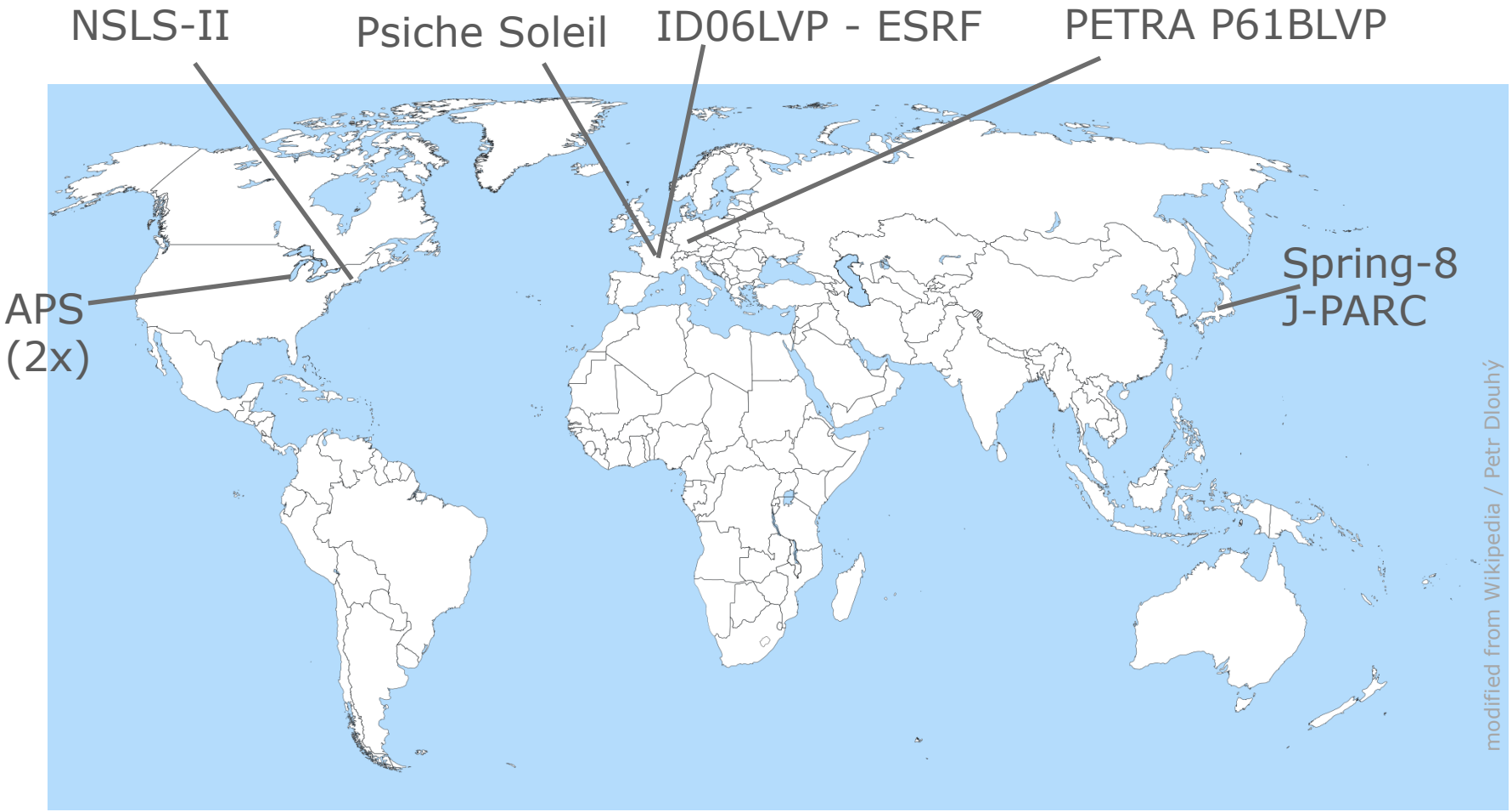

Large volume presses

LVP – ID06 ESRF

In-situ properties under HP-HT

- ❑ Phase stabilities (solid, melting…)
- ❑ Kinetics of reactions
- ❑ Viscosity
- ❑ Strength, brittle behavior
- ❑ Electric conductivity P-T dependence
- ❑ Elastic properties
- ❑ Melt properties (density, etc.)
- ❑ Thermal diffusivity

…

Large volume presses

LVP – ID06 ESRF

- Large volume (mm^3): statistics !
- Small P and T gradients
- Stable P and T over days
- Investigate grain size dependences
- Tunability of the cell assemblies

BUTs

- no easy access to sample
- hours for loading-unloading stages
- T & P limited compared to DAC.

Main synchrotron X-ray probes with multi-anvil

- X-ray imaging

- X-ray diffraction

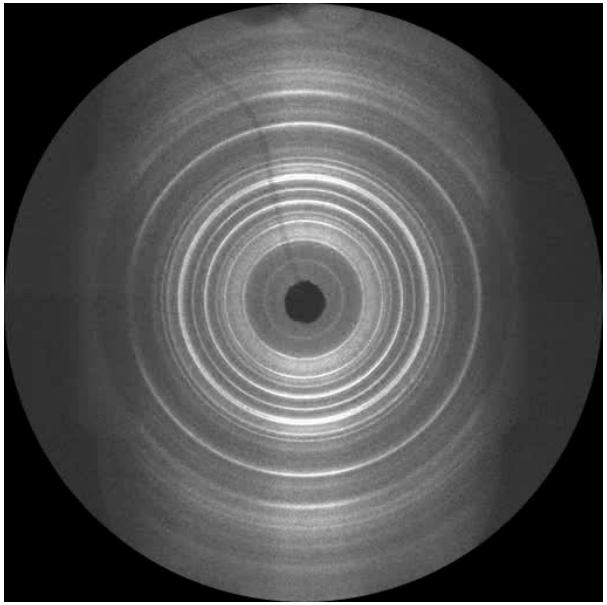

Beamline basic setup: imaging + diffraction

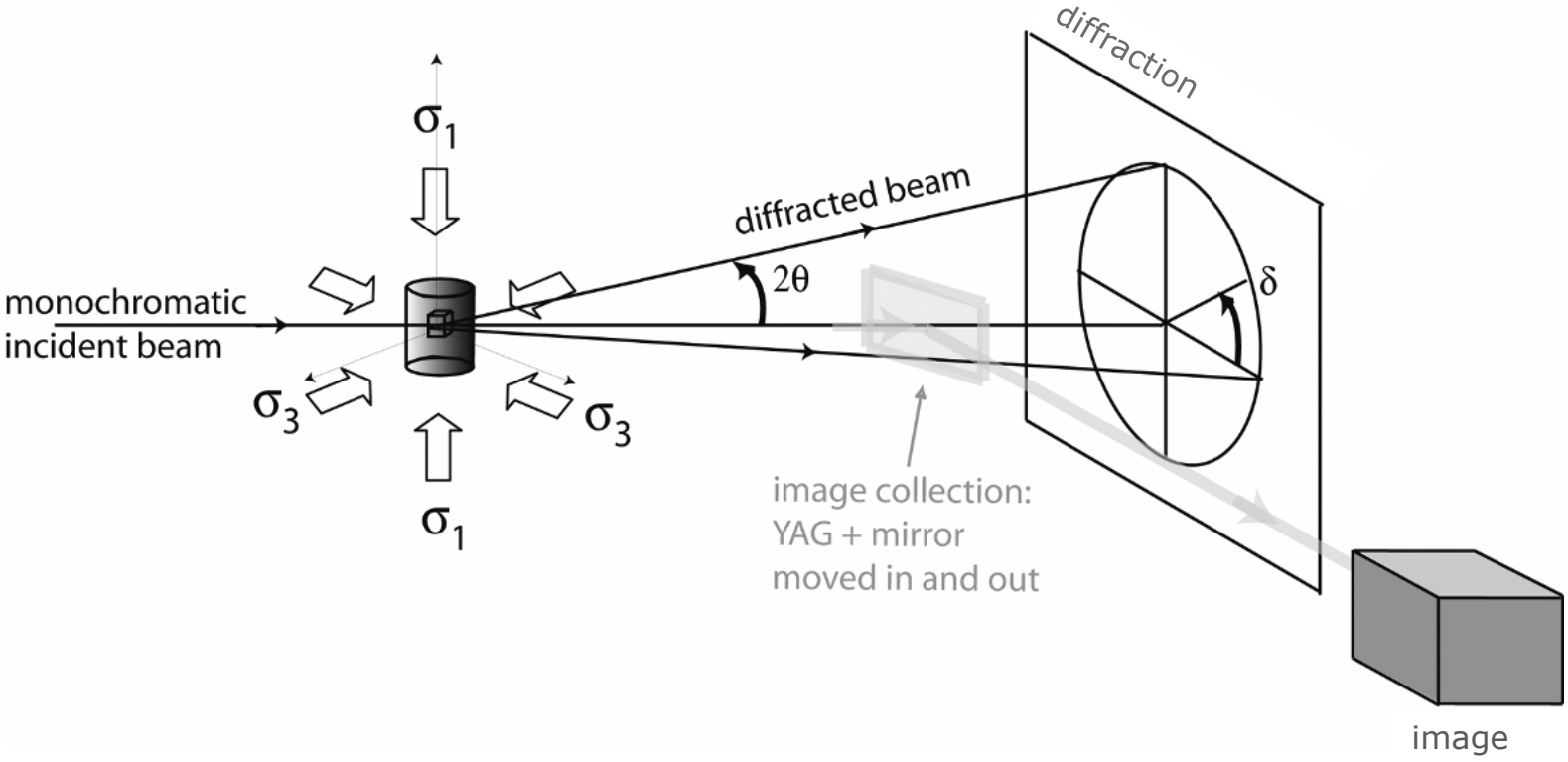

High-pressure, large volume x-ray ‘transparent’ environment: octahedric assemblages

Anvils:

- All WC
- cBN
- Sintered diamond
- …

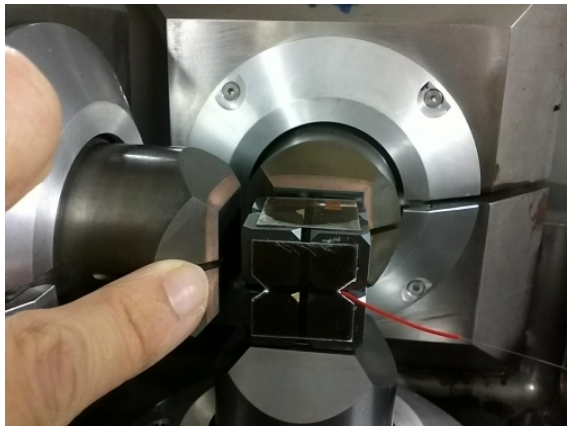

www.synchrotron-soleil.fr

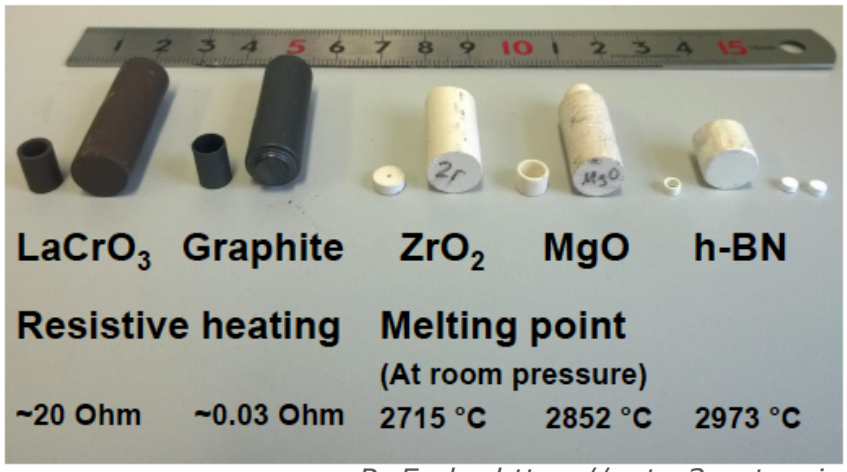

R. Farla, https://petra3-extension.desy.de

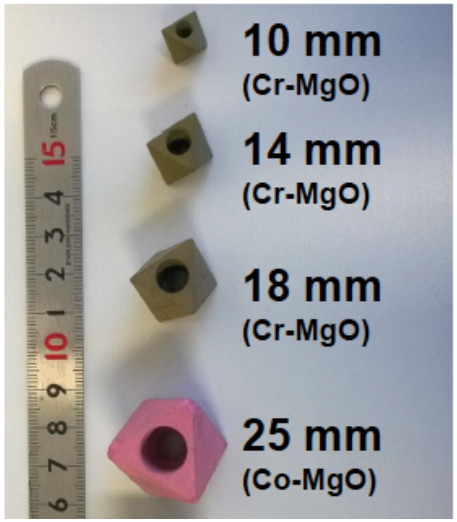

High-pressure, large volume x-ray 'transparent' environment: beam vs. cell assembly

white beam

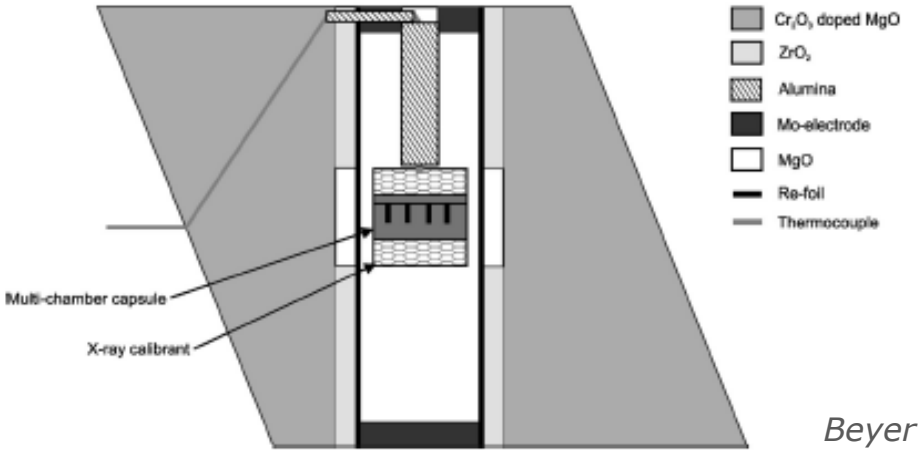

monochromatic beam

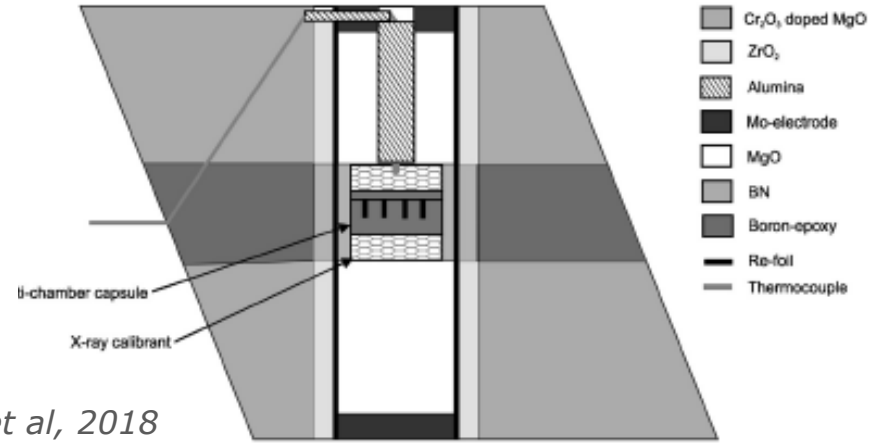

Beyer et al, 2018

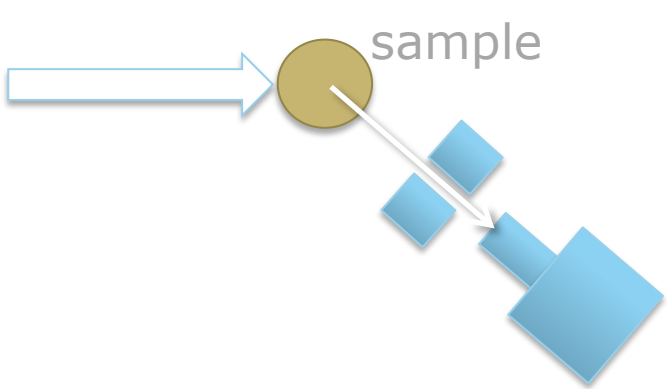

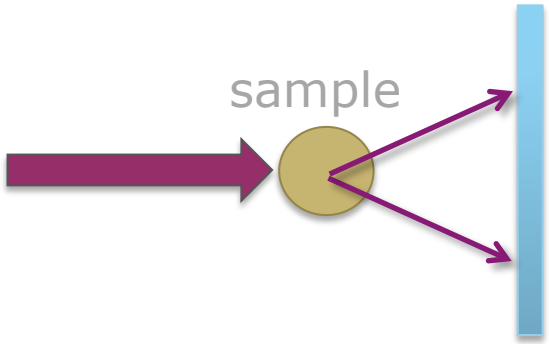

High pressure, large volume x-ray 'transparent' environment: cubic assemblages

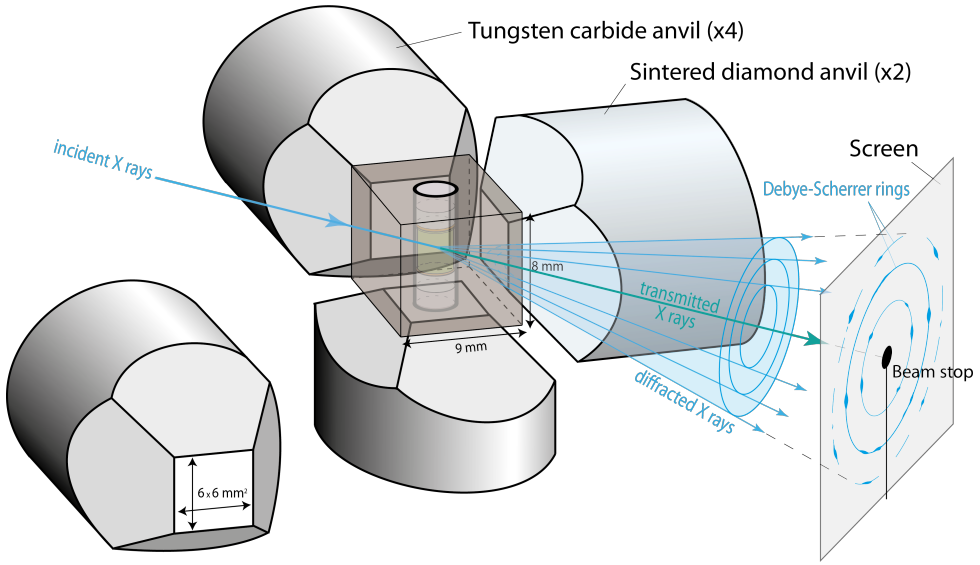

T. Ferrand 2017

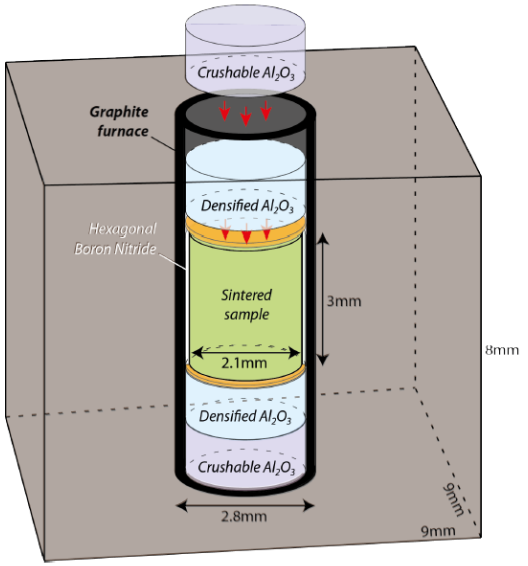

T. Ferrand 2017

Anvils:
- cBN
- Sintered diamond
- ...

Pressure transmitting medium:
- amorphous Boron + epoxy
- fired pyrophyllite (cube or bone-dry sphere)
- Cr,Co doped MgO

!! am. B-epoxy windows if mono beam

Furnaces: graphite

On temperature gradients vs. cell material

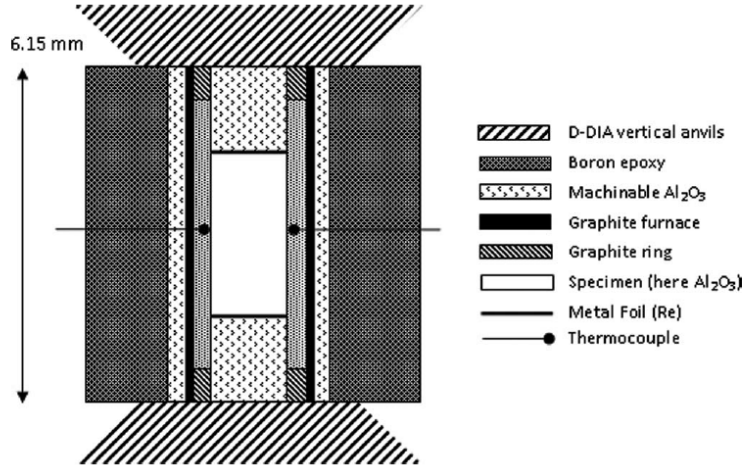

Al_2O_3 κ = 6 to 8 $W.m^{-1}K^{-1}$ (1100K-1700K)

Raterron et al, RSI 2013: using XRD, gradient up to 150 K / mm

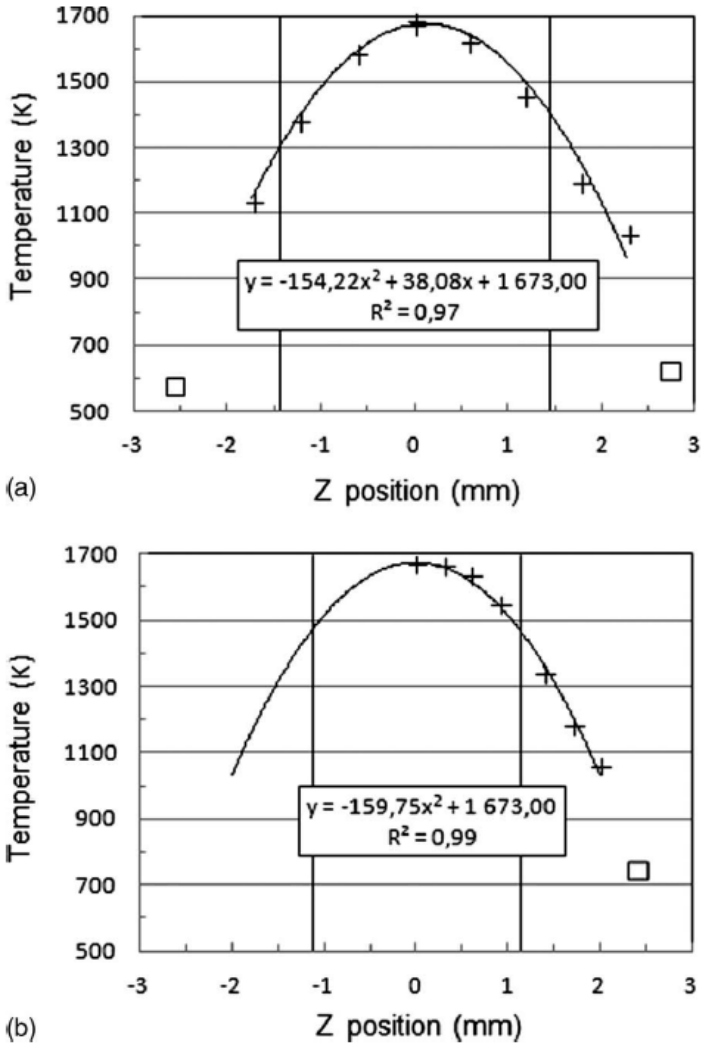

On temperature gradients vs. cell material

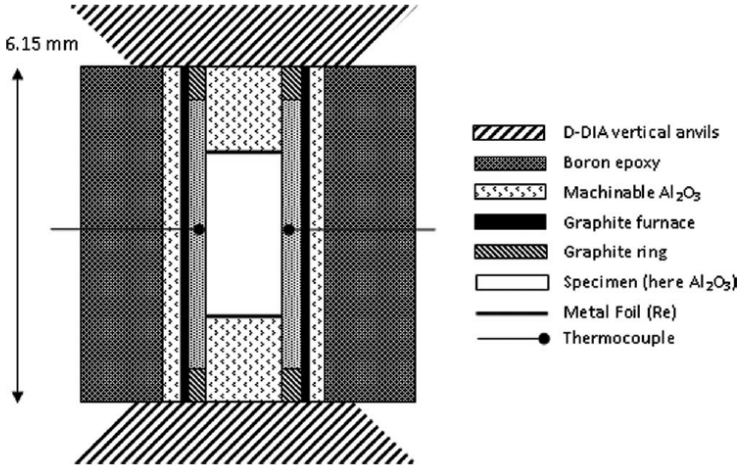

Al_2O_3 κ = 6 to 8 $W.m^{-1}K^{-1}$ (1100K-1700K)
YSZ ($Y\text{-}ZrO_2$) : κ = 2 $W.m^{-1}K^{-1}$ (1300 K)

Raterron et al, RSI 2013: using XRD, gradient up to 150 K / mm

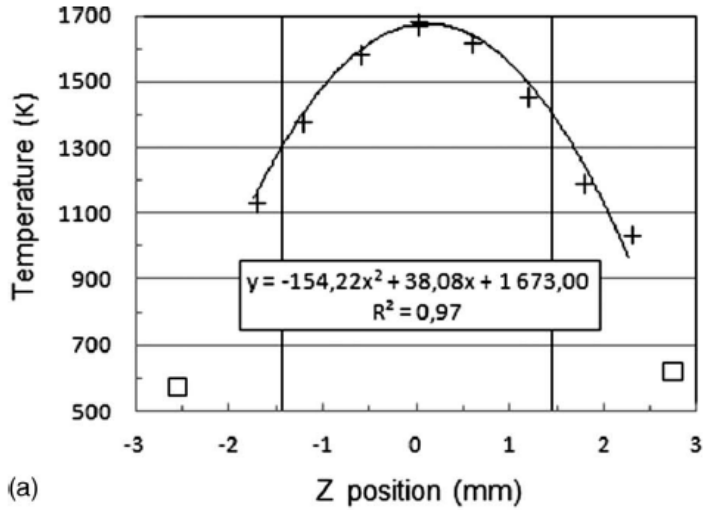

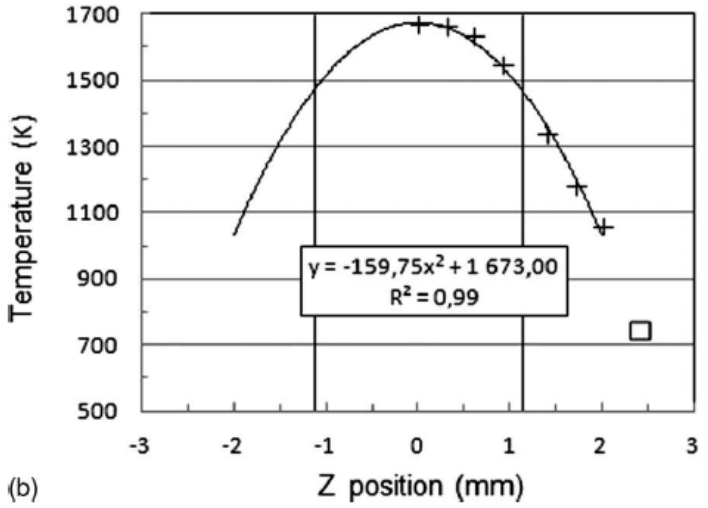

On high temperatures and mechanical stability of a LVP cell

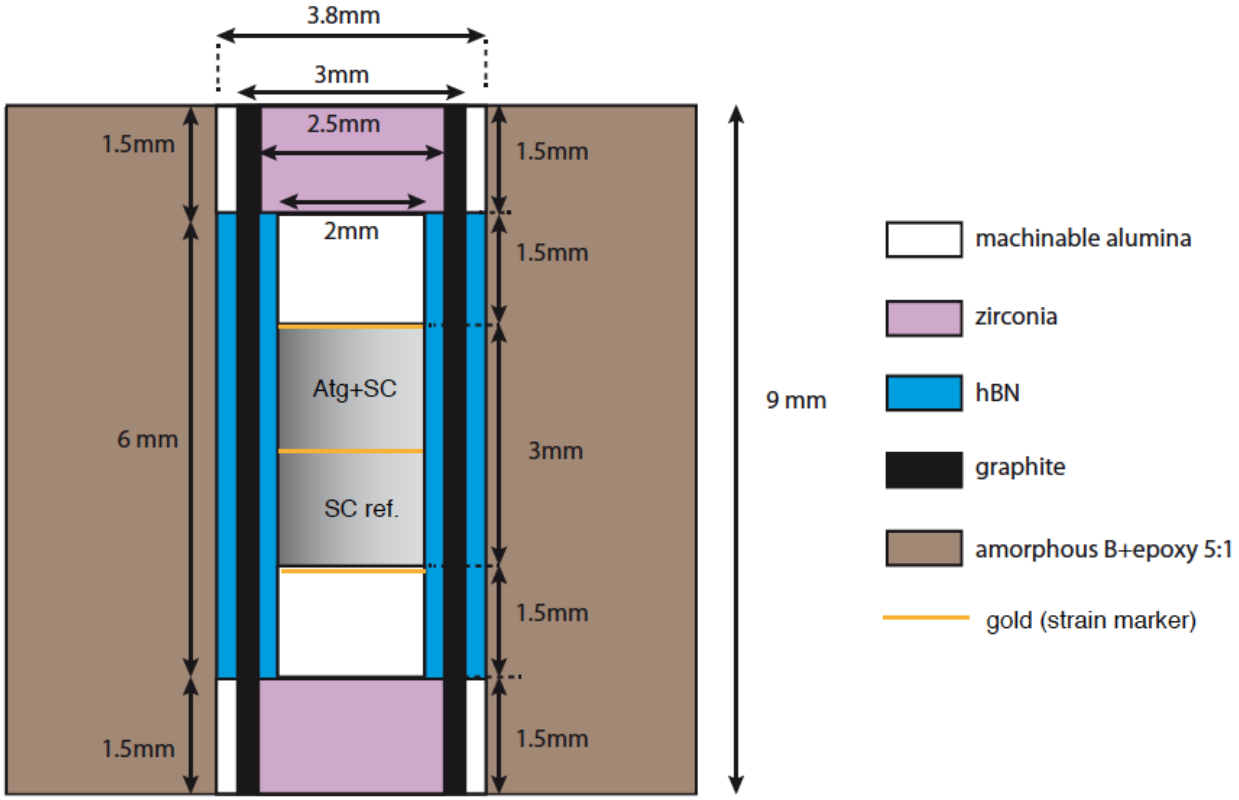

LVP for deformation

synchrotron XRD raised a major obstacle for deformation studies under HP :
above pressures of 2 GPa frictions at too high to use conventional stress gauges.

High-pressure environment for deformation: D-DIA

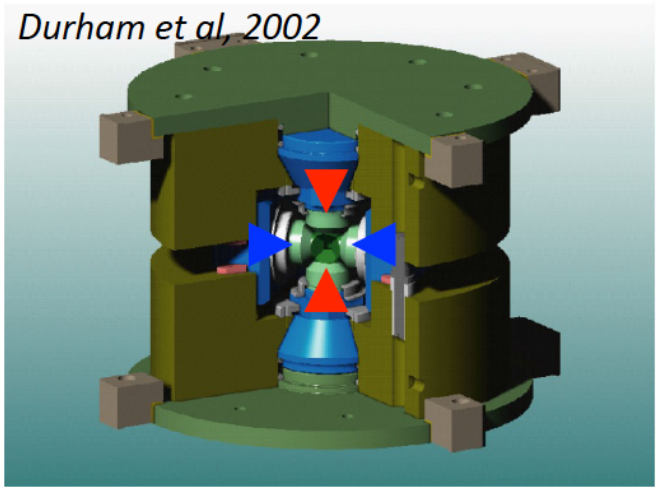

constant volume deformation at HP-HT (20GPa, 1800K)

In-situ properties under HP-HT + stress

- viscosity, strength
- deformation mechanisms, defects
- Transformation mechanisms under stress
- electric or elastic properties vs. crystal preferred orientation, ⋯

High-pressure environment for deformation: D-DIA

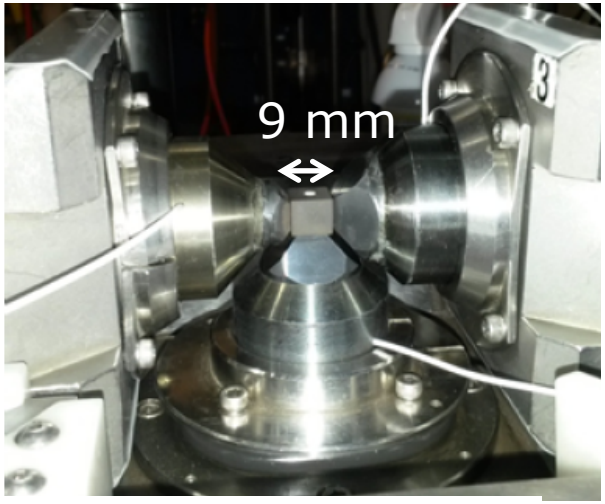

D-Dia 'simple stage'
APS GSECARS

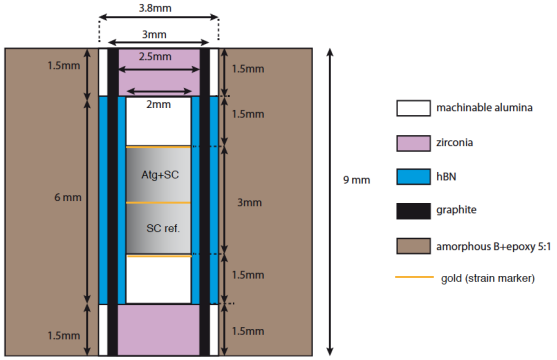

Nishiyama et al, 2008, Kawazoe et al, 2009

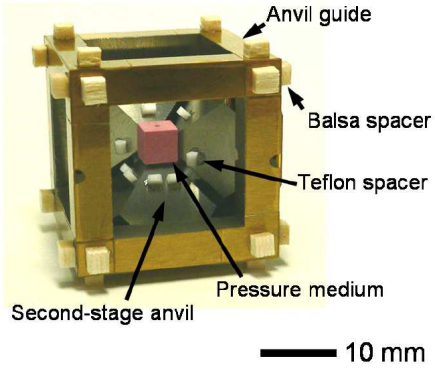

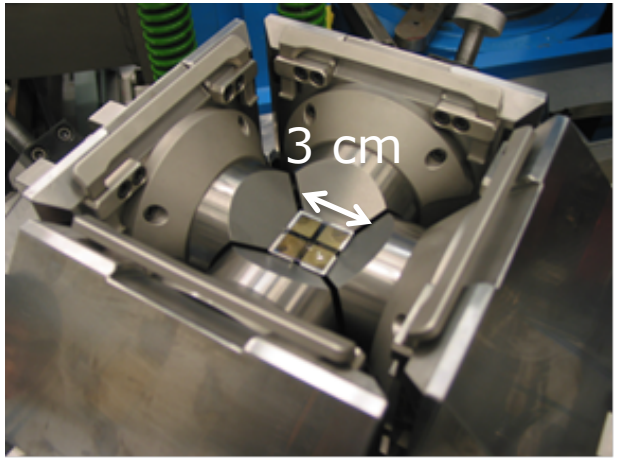

D-Dia double-stage, APS

Opposed anvils configurations: Rotational Drickamer Apparatus (RDA)

Yamazaki and Karato, 2001

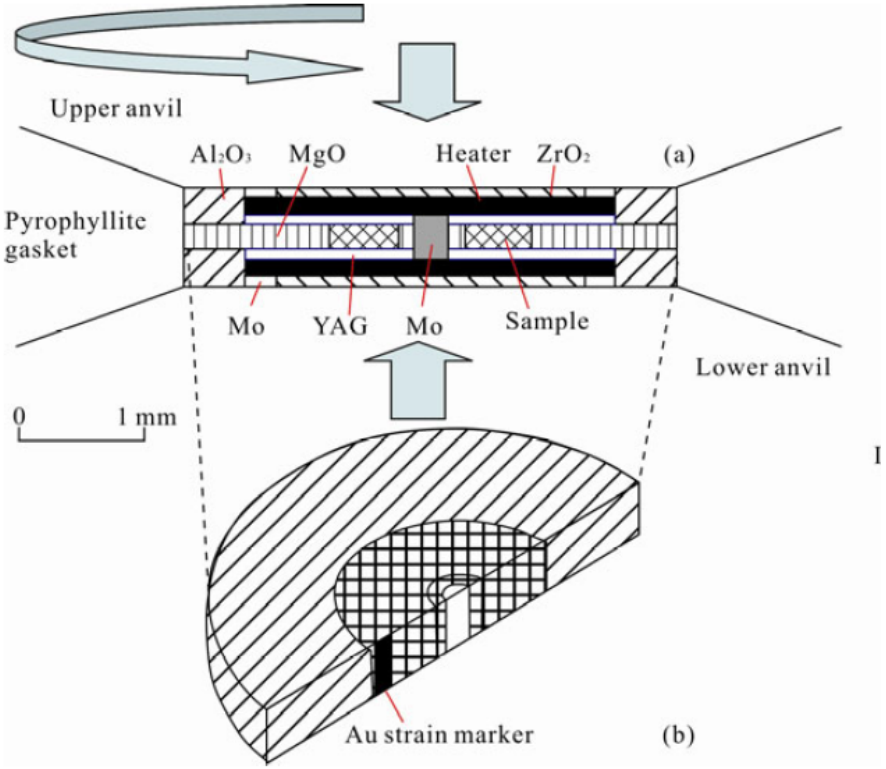

- Portable. Mostly operated at NSLS.
- 25 GPa, 2000 K

Opposed anvils configurations: High Pressure X Tomography Microscope (HPXTM)

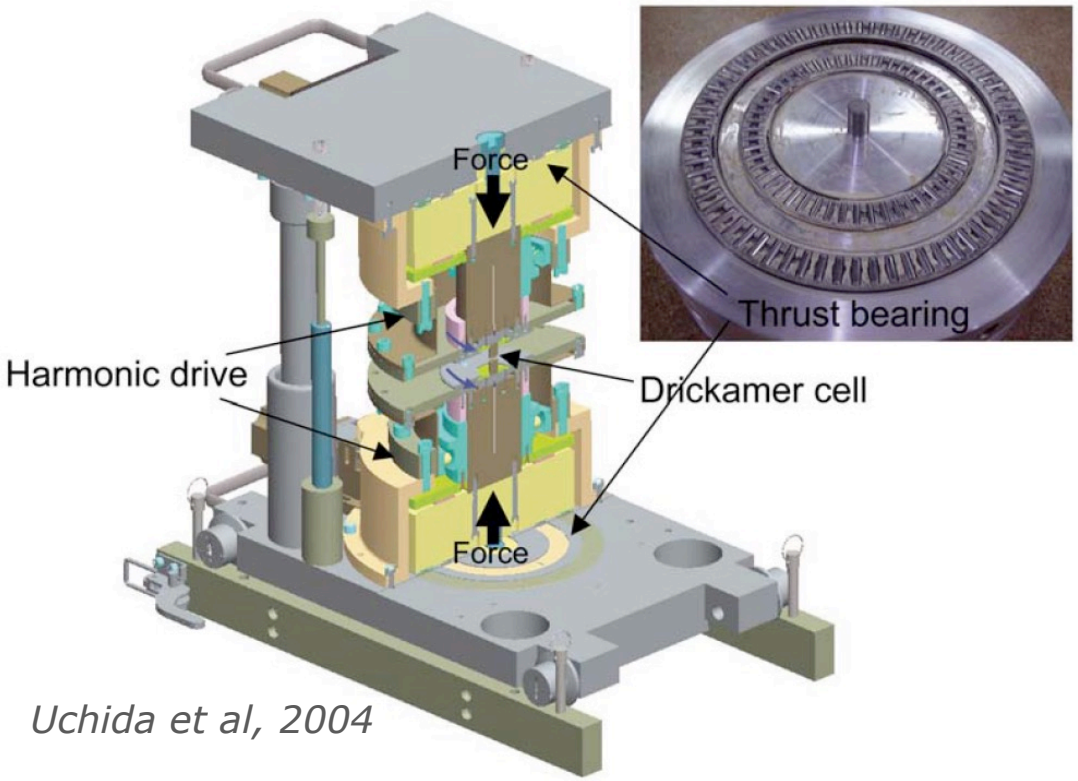

Uchida et al, 2004

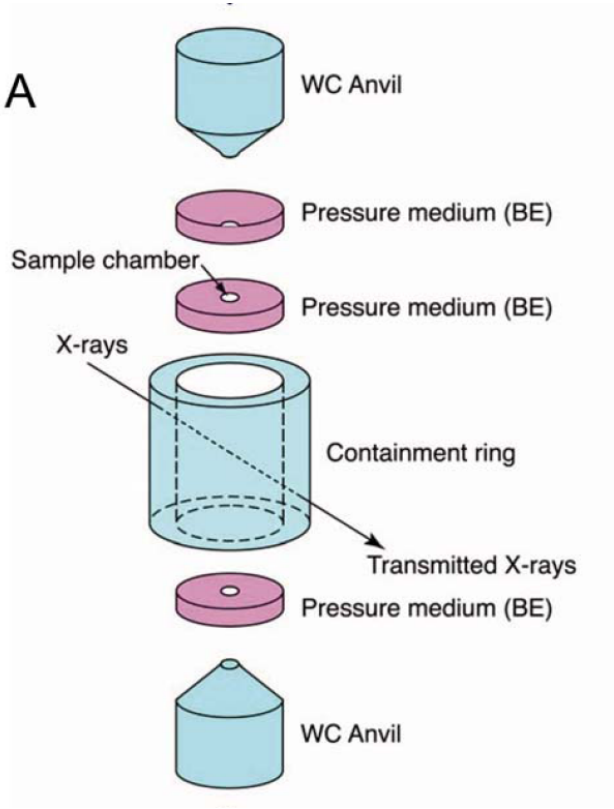

- Specificity : large volume.
- 8-10 GPa.

LVP and synchrotron x-ray data

X-ray imaging

absorption contrast

- track boundaries and objects (deformation, diffusivity…), objects, densities … (more: J-P. Perrillat and Y. Le Godec's talks)
- measure length (V_P-V_S at high P-T)
- cross-correlation on image pairs (sub-pixel, complex geometries)

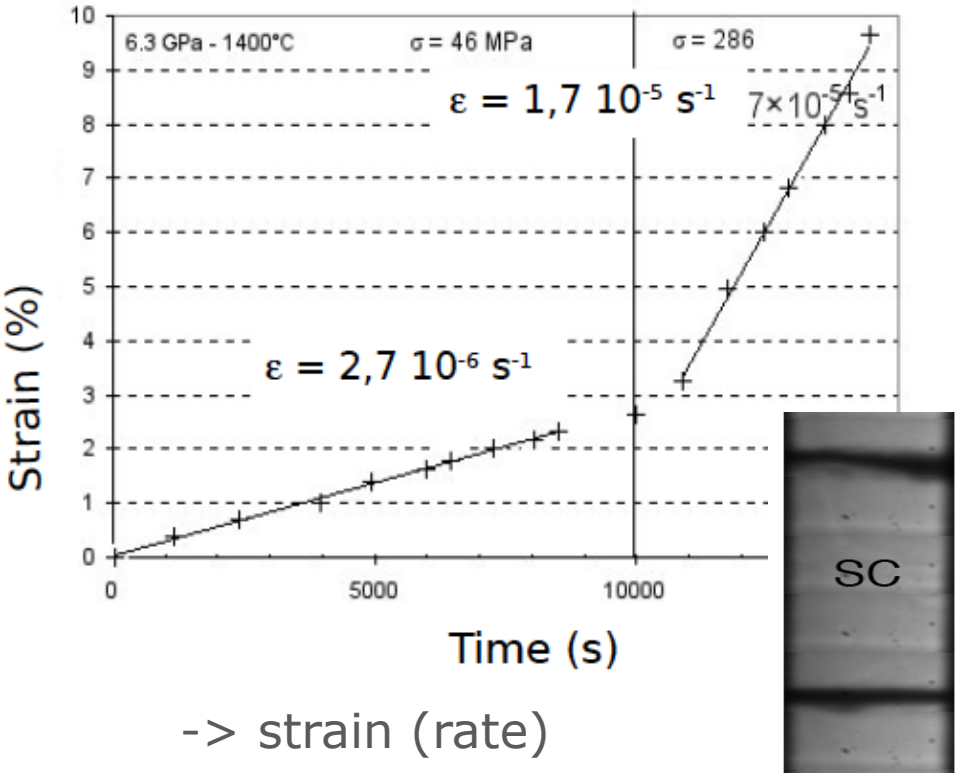

-> strain (rate)

P. Raterron

X-ray imaging

Mineralogical Magazine, October 2011, Vol. 75(5), pp. 2597–2610

The effect of pressure on thermal diffusivity in pyroxenes

S. A. HUNT[1,2,3,*], A. M. WALKER[4], R. J. MCCORMACK[2], D. P. DOBSON[2], A. S. WILLS[3] AND L. LI[1]

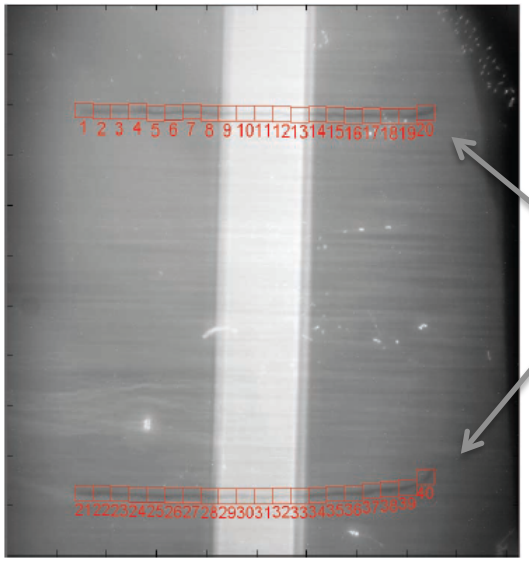

X-ray imaging

Mineralogical Magazine, October 2011, Vol. 75(5), pp. 2597–2610

The effect of pressure on thermal diffusivity in pyroxenes

S. A. Hunt[1,2,3,*], A. M. Walker[4], R. J. McCormack[2], D. P. Dobson[2], A. S. Wills[3] and L. Li[1]

➔ $\kappa = f(P, T)$

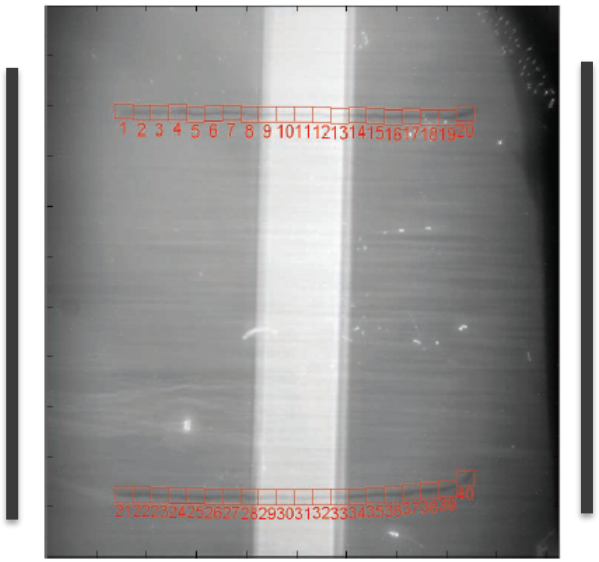

Sine-wave on furnace:
+-30 to 50°C

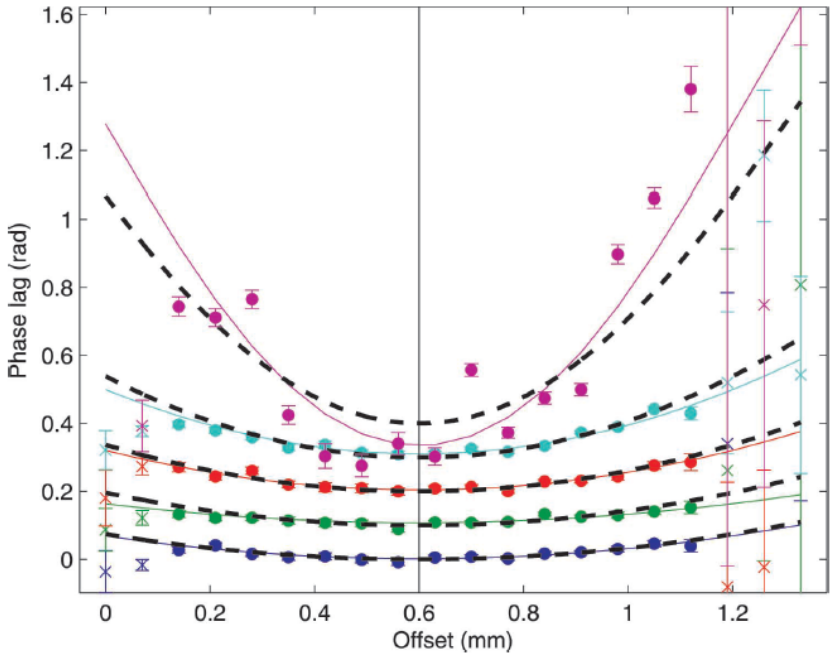

Diffraction

JOURNAL OF GEOPHYSICAL RESEARCH, VOL. 117, B06209, doi:10.1029/2011JB009100, 2012

_P-V-T_ equation of state of stishovite up to mid-lower mantle conditions

Fulong Wang,[1] Yoshinori Tange,[1] Tetsuo Irifune,[1] and Ken-ichi Funakoshi[2]

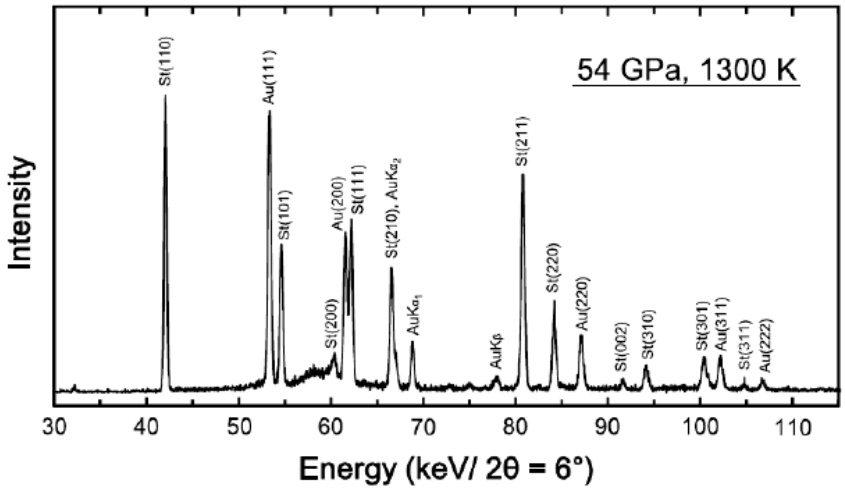

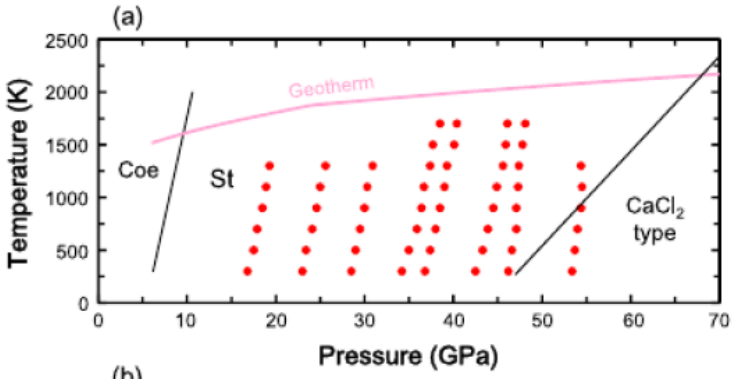

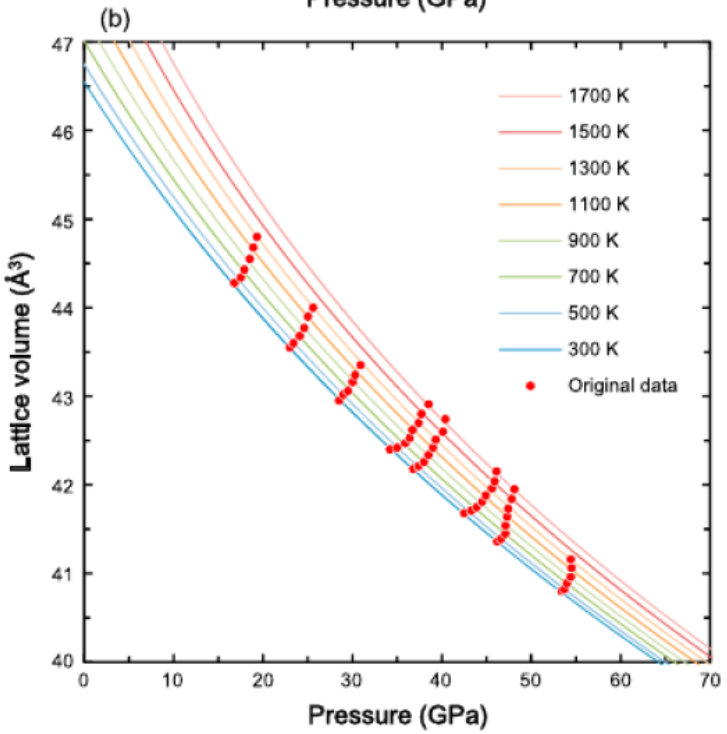

LVP and x ray data for in situ deformation

Or how stress shows up in x-ray diffraction (polycrystal)

X-Ray diffraction : under high pressure

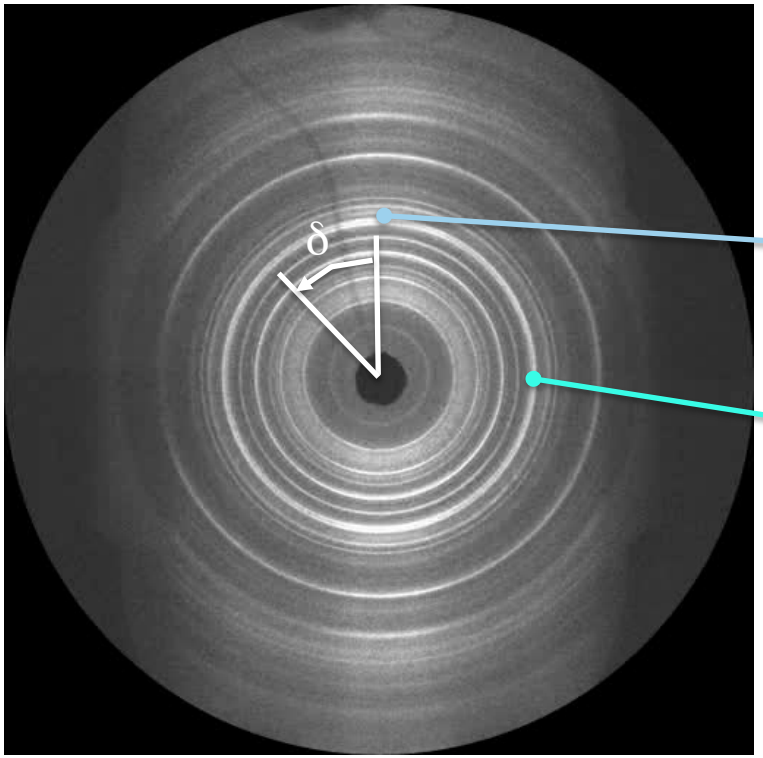

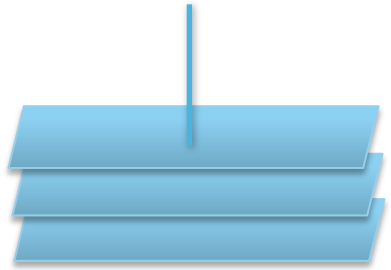

δ = 0°

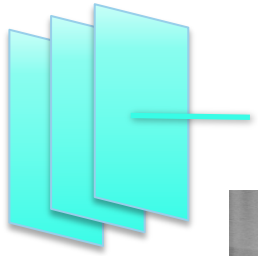

δ = 90°

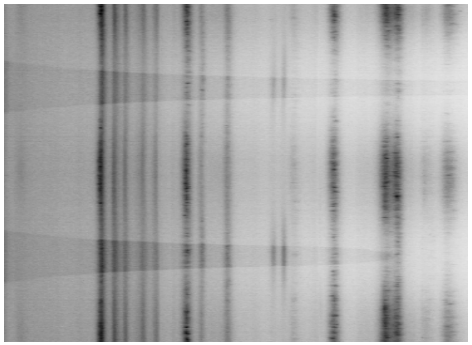

X-Ray diffraction : under high pressure + non hydrostatic stress

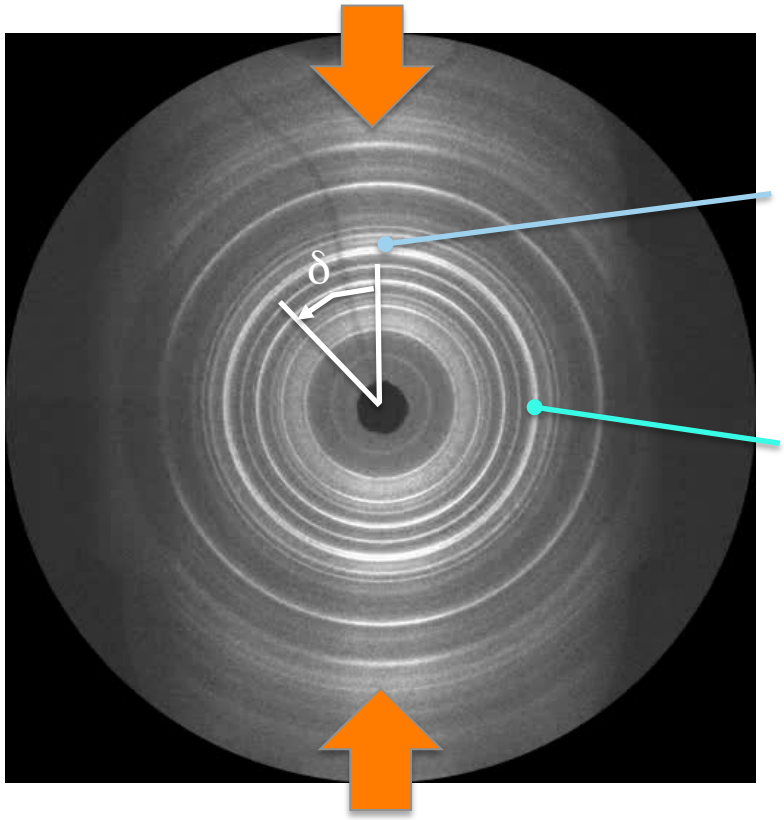

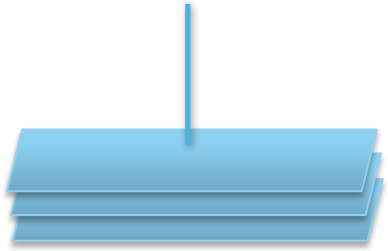

δ = 0°

« lattice strain »

δ = 90°

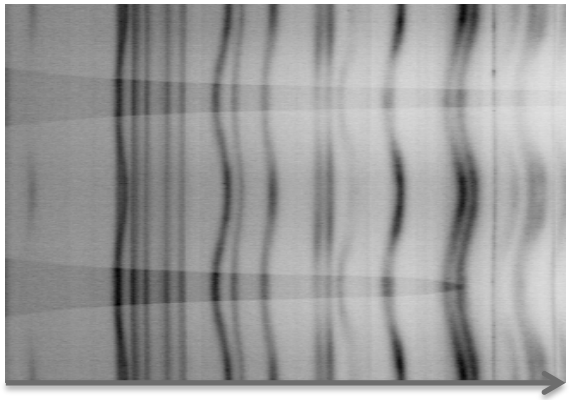

Stresses under high pressure (uniaxial)

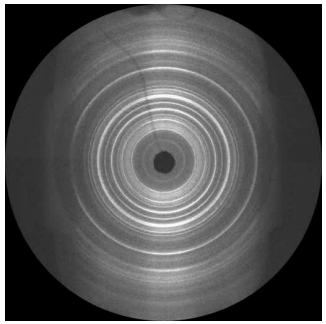

$$\sigma_{ij} = \begin{vmatrix} \sigma_{11} & 0 & 0 \\ 0 & \sigma_{11} & 0 \\ 0 & 0 & \sigma_{33} \end{vmatrix} = \begin{vmatrix} \sigma_P & 0 & 0 \\ 0 & \sigma_P & 0 \\ 0 & 0 & \sigma_P \end{vmatrix} + \begin{vmatrix} -t/3 & 0 & 0 \\ 0 & -t/3 & 0 \\ 0 & 0 & 2t/3 \end{vmatrix}$$

deviatoric stress

σ_P : mean stress = « hydrostatic pressure » = P

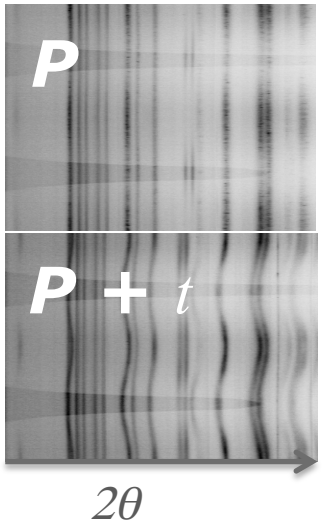

***P* and *t* can be obtained simultaneously and for each phase**

Stresses under high pressure (uniaxial)

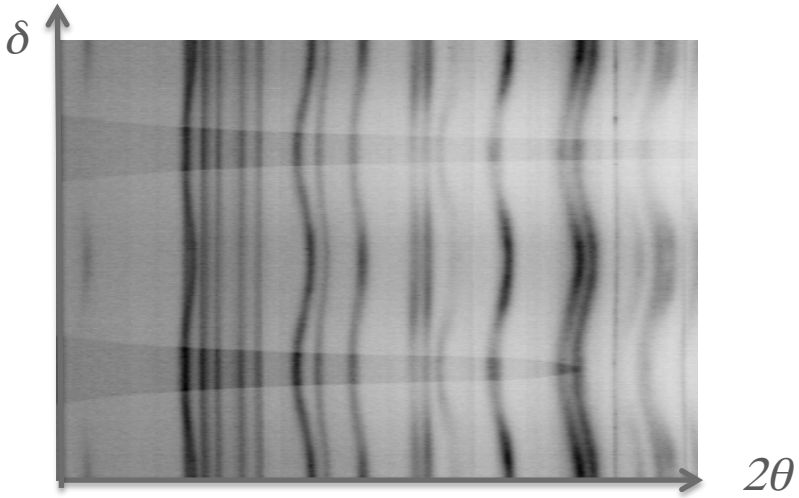

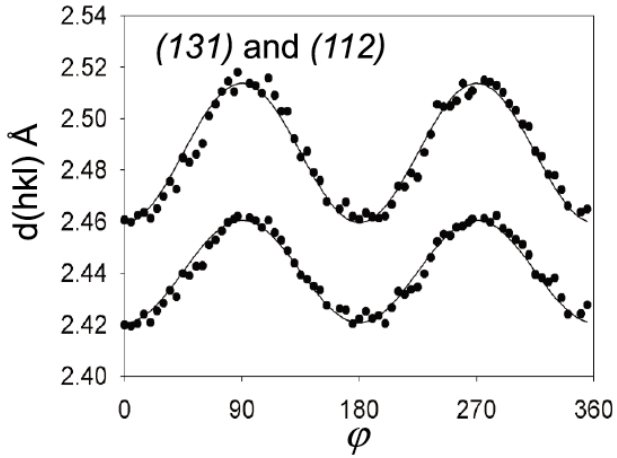

with $\cos\phi = \cos\delta.\cos\theta$

$$\frac{d_{(hkl)}(\varphi) - d_{P(hkl)}}{d_{P(hkl)}} = Q_{(hkl)}(1 - 3\cos^2\varphi)$$

pressure:
equation of state

Lattice strain
-> stress with *Cij*

Singh et al, 1998, Uchida et al, 1996
Multifit-Polydefix, Merkel and Hilairet, 2015.

Stresses under high pressure (uniaxial)

$$t(hkl) = 6Q(hkl)G(hkl)$$

G(hkl) from the *Cij*.
elastic theory,
Singh et al, 1998, Uchida et al, 1996

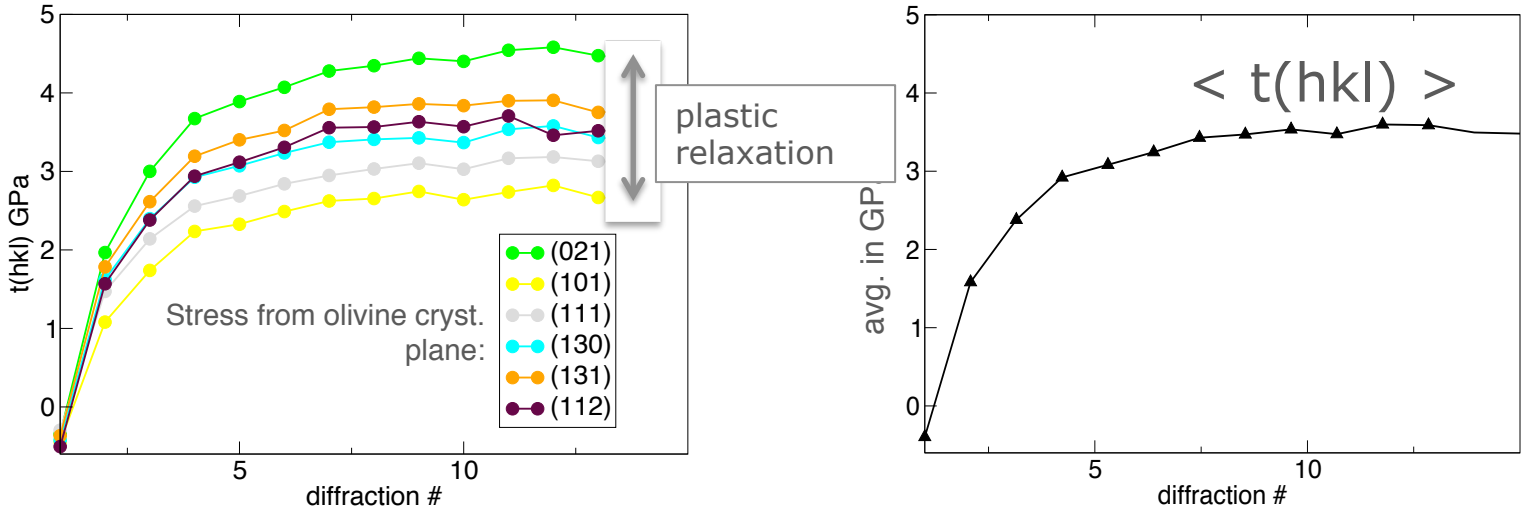

< t(hkl)> = non-hydr. stress on sample ?
Not so simple.
Models are necessary to calculate absolute stresses.

Energy Dispersive configuration (NSLS, APS ID6)

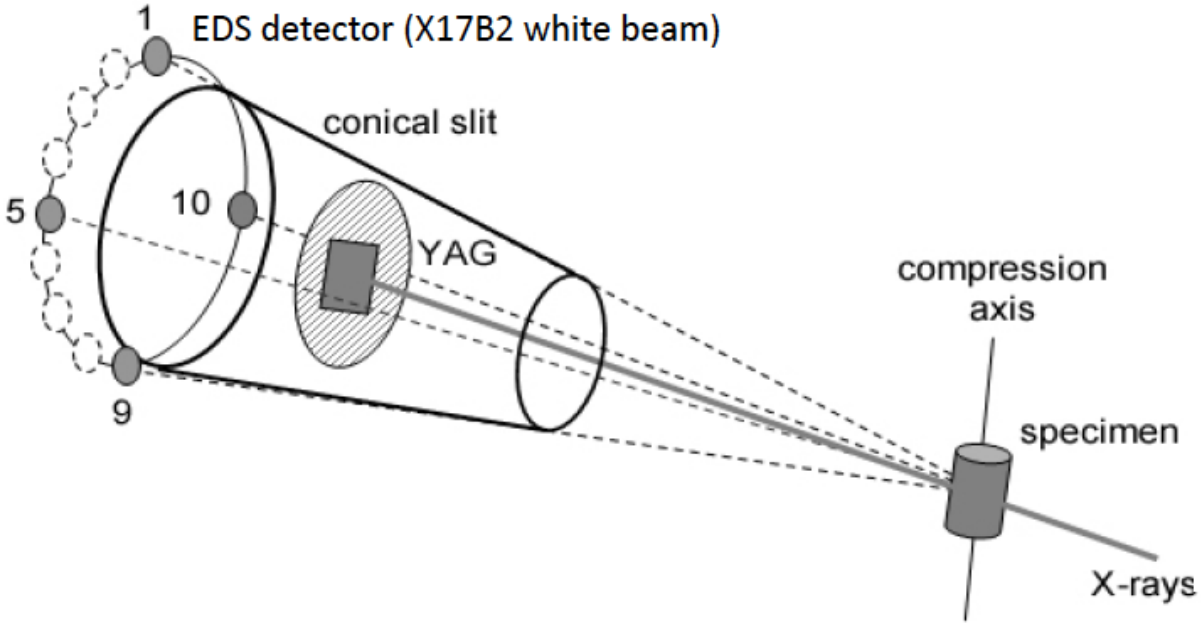

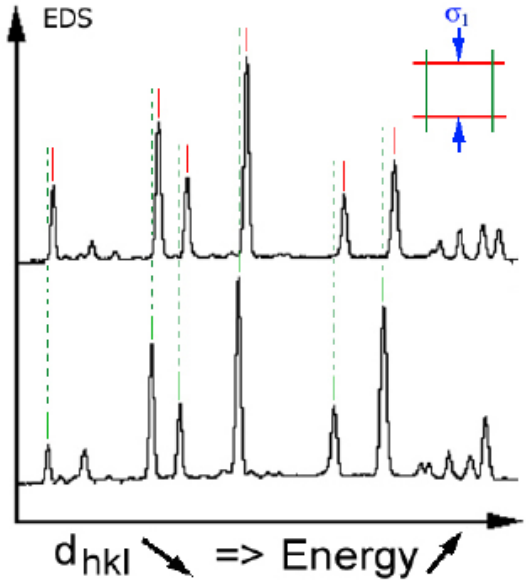

X-Ray diffraction : stresses under high pressure

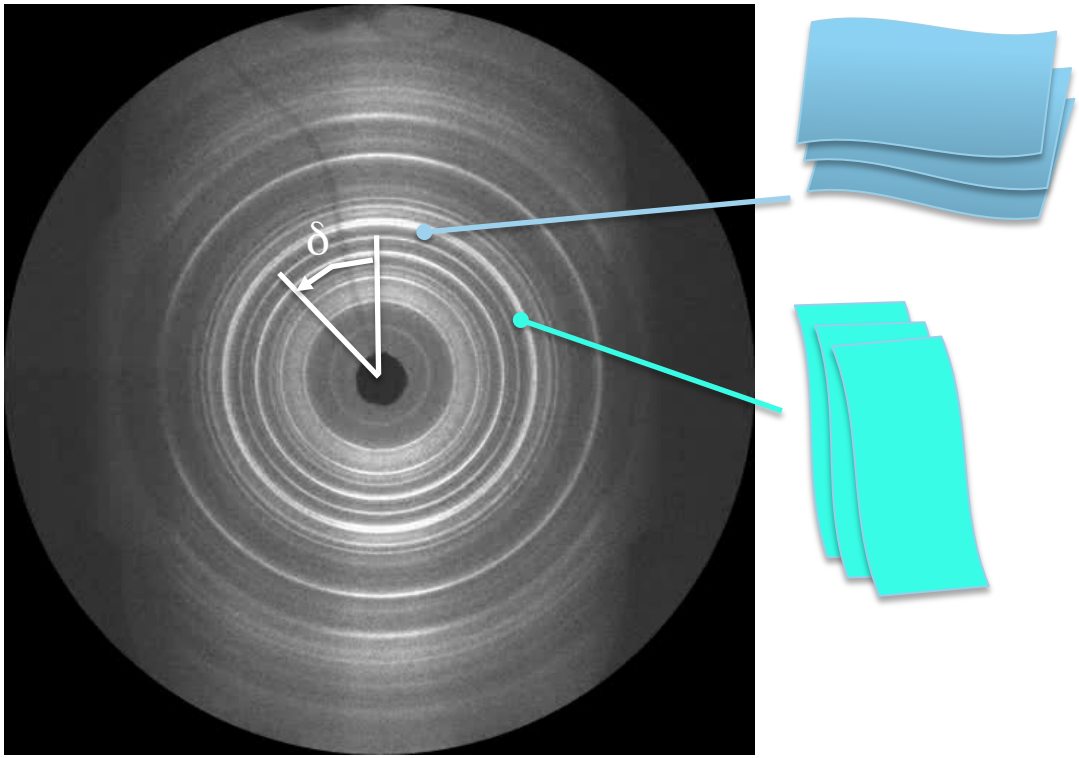

local lattice strains
(crystal to crystal and
intra-crystalline)
-> peak broadening

Case study : stress partitionning in two-phases aggregates under HPT

multi-phase polycrystal deformation

load bearing frame
controlled by strong phase

interconnected weak layer
controlled by weak phase

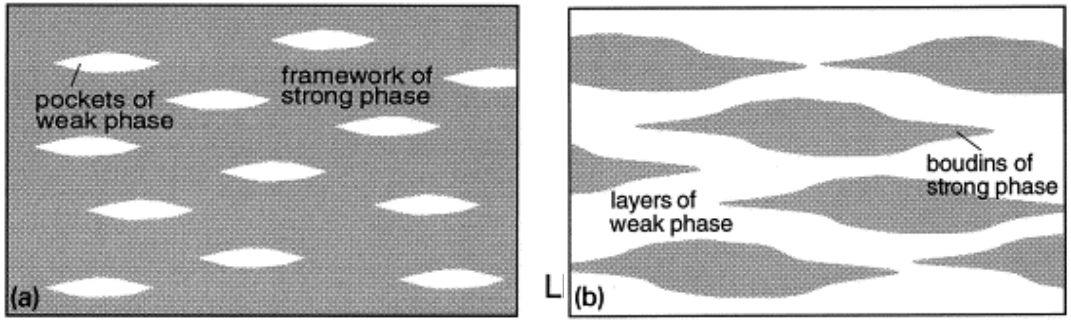

Handy, 1994

Increasing strain

Increasing weak phase amount

- Which material is the weakest / strongest?
- How do stress and strain partition in the phases?
- [What is the viscosity of the aggregate ?]

Serpentine + olivine aggregates deformation at 300-350°C, 3 to 4 GPa, ca. $2.10^{-5}s^{-1}$

varying weak phase content (5 to 50%)
compare to pure phase

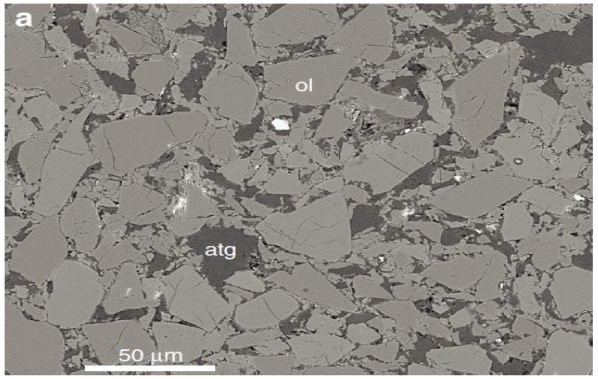

Saturday night fever at ID06@ESRF!

Serpentine + olivine aggregates deformation at 300-350°C, 3 to 4 GPa, ca. $2.10^{-5}s^{-1}$

varying weak phase content (5 to 50%)
compare to pure phase

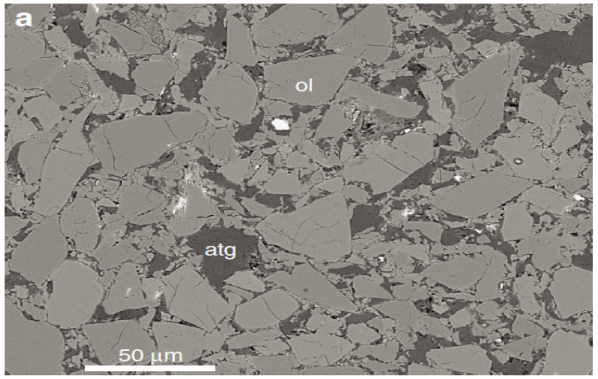

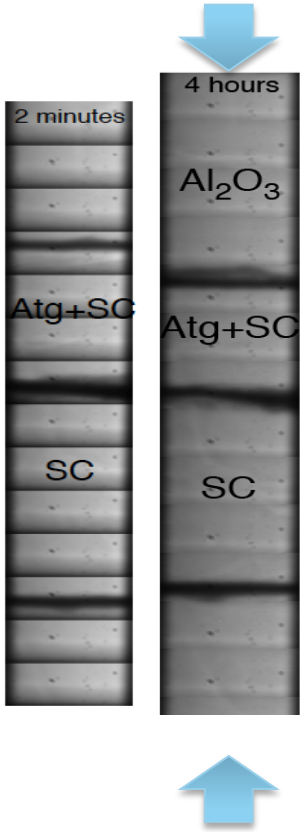

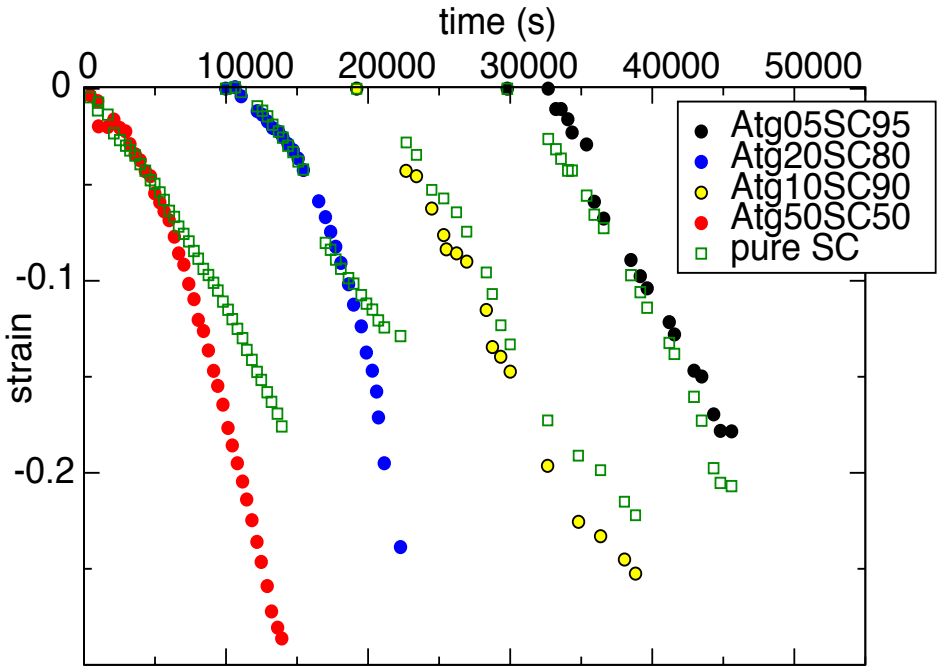

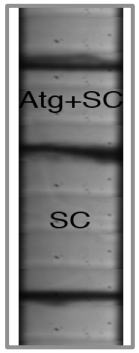

Serpentine+olivine aggregates deformation at 300-350°C, 3 to 4 GPa, ca. $2.10^{-5}s^{-1}$

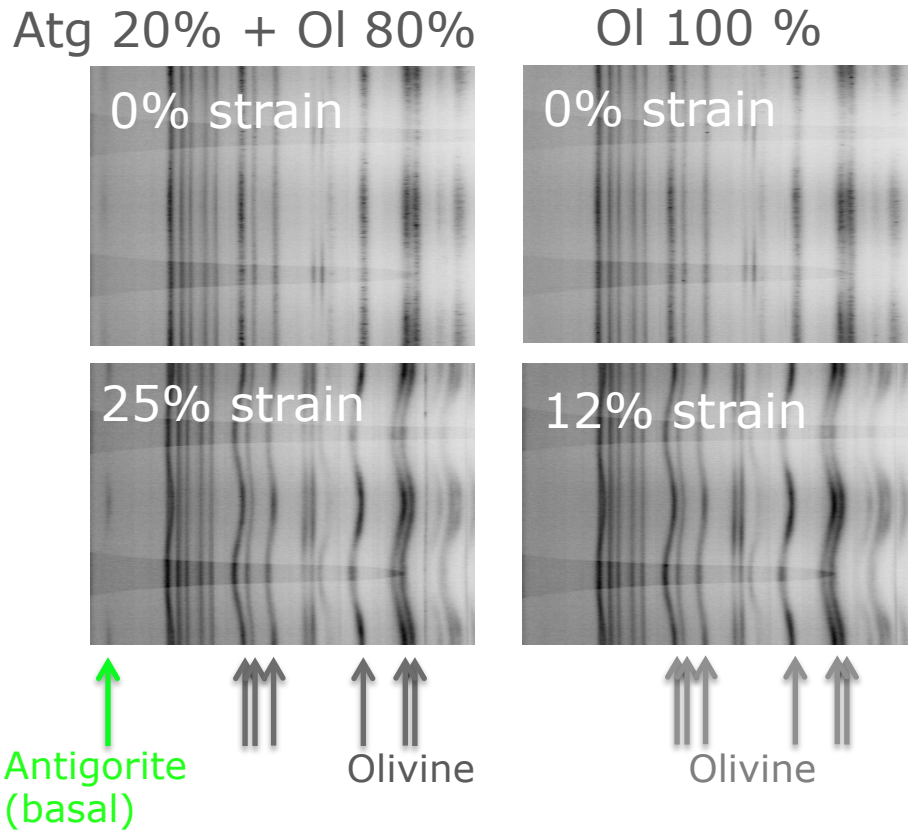

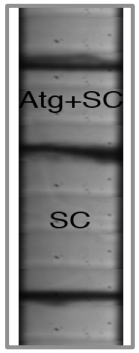

Serpentine+olivine aggregates deformation at 300-350°C, 3 to 4 GPa, ca. $2.10^{-5}s^{-1}$

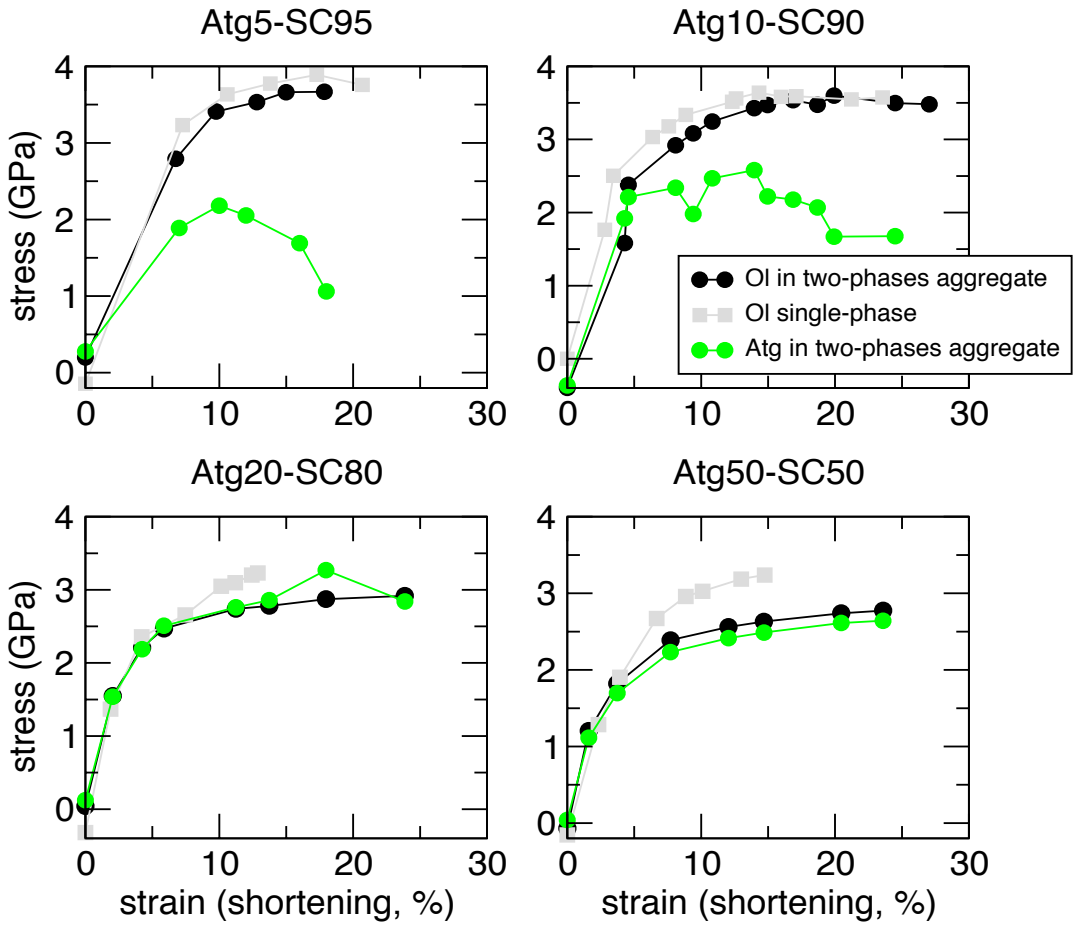

Up to 10% vol, weak phase is shielded by load bearing frame

If 20% or more, weak phase has an effect

LVP and x ray data for in situ deformation

x-ray diffraction under stress: crystal preferred orientations ?

X-Ray diffraction : crystal preferred orientations in a polycrystal under high pressure

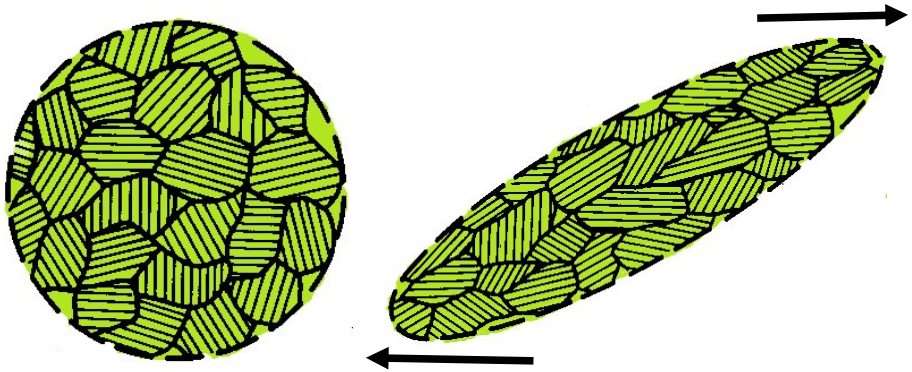

Plastic deformation
Dislocation glide
Grain rotations
Non-random crystal orientations

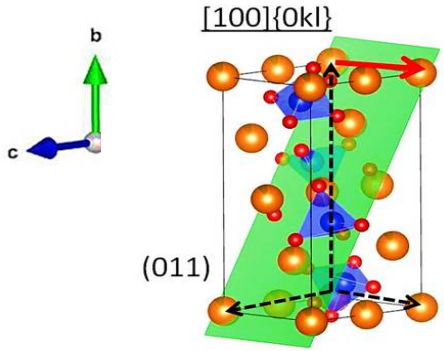

Olivine - example of slip system

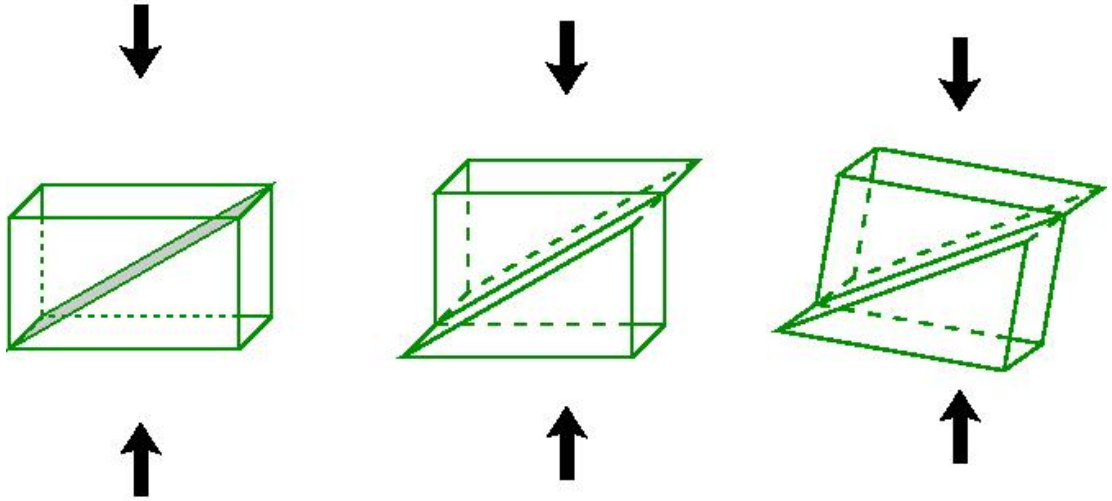

images S. Merkel

X-Ray diffraction : crystal preferred orientations in a polycrystal under high pressure

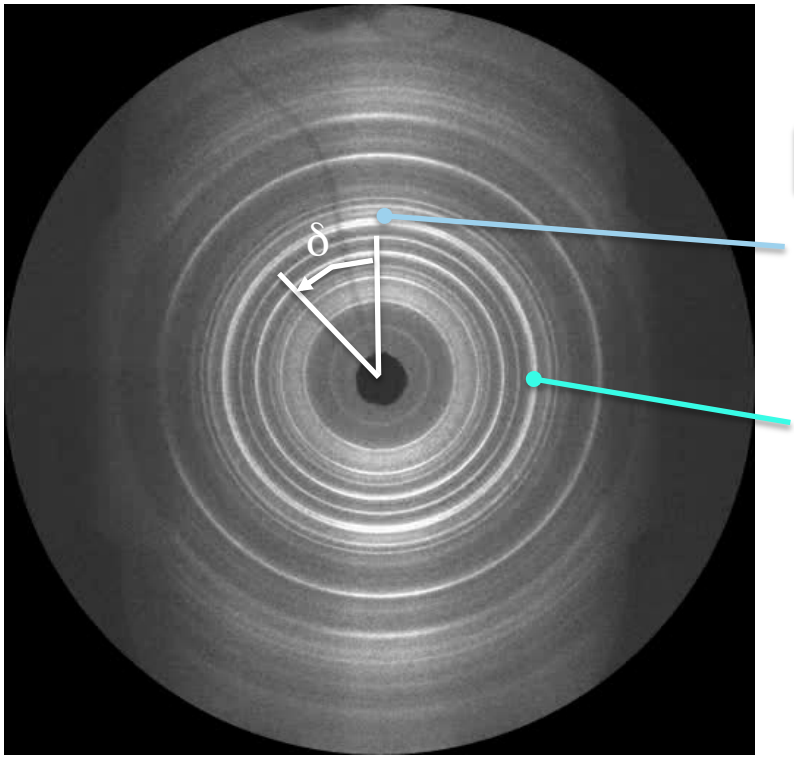

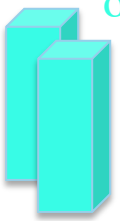

intensity variations
→ CPO, « texture »

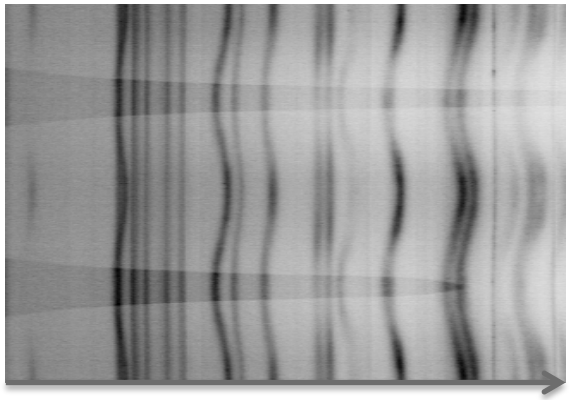

X-ray diffraction for microstructure

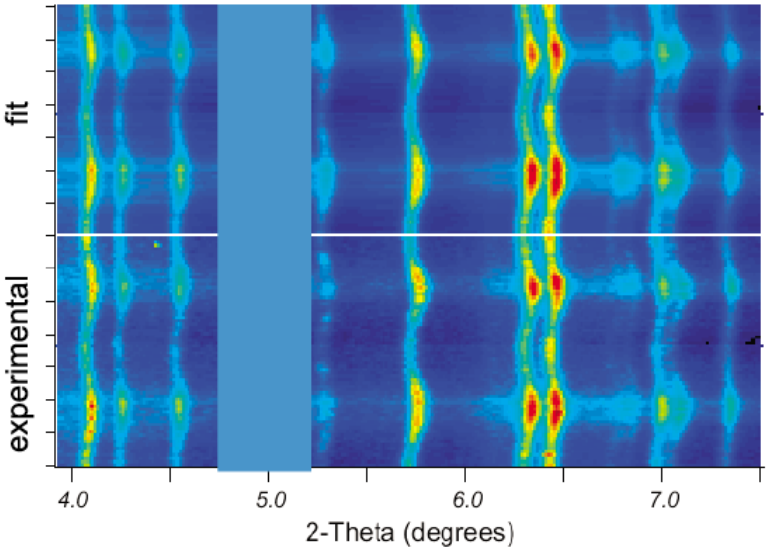

Texture analysis

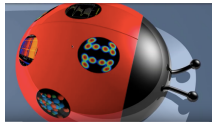

MAUD software
http://www.ing.unitn.it/~maud/
L. Lutterotti

inverse pole figure = probability to find a direction of interest, here the maximum compression direction, in the crystal coordinates system

olivine at 5 GPa 1600K, strain 11% orthorhombic

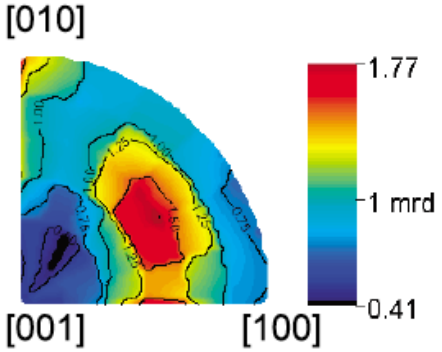

X-ray diffraction for microstructure

ε-Fe deformed to 11% at 17 GPa, 400K, ca. 10^{-5} s^{-1}

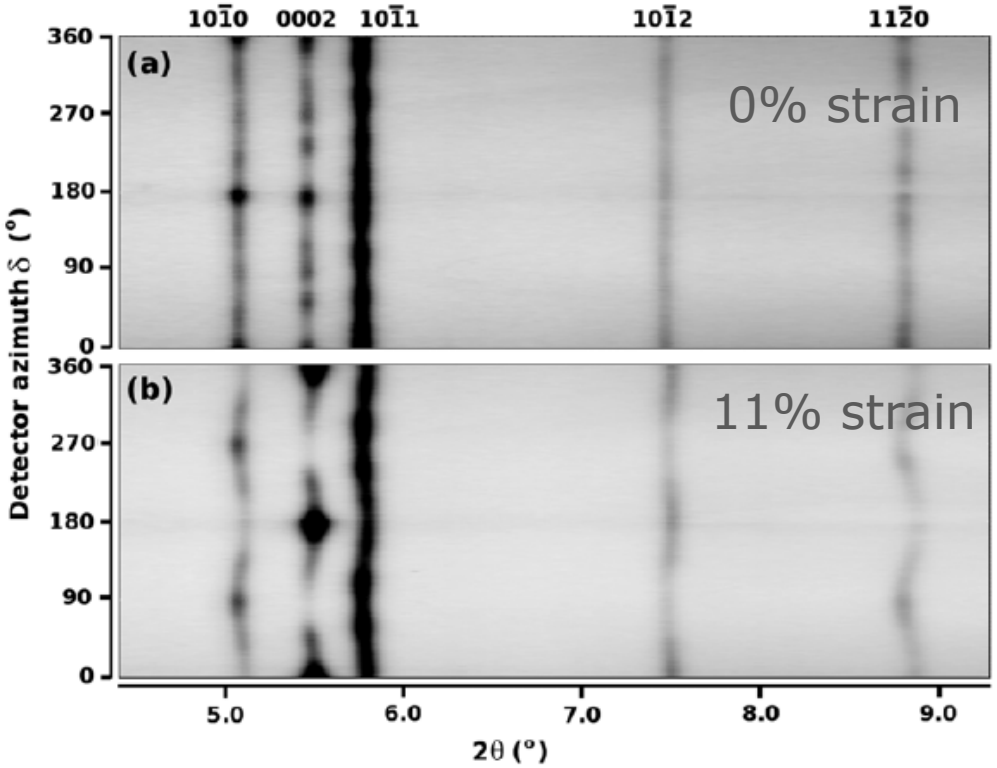

Nishiyama et al, Geophys. Res. Lett., 2005
Merkel et al, Model. Sim. Mater. Sc. Eng. 2012

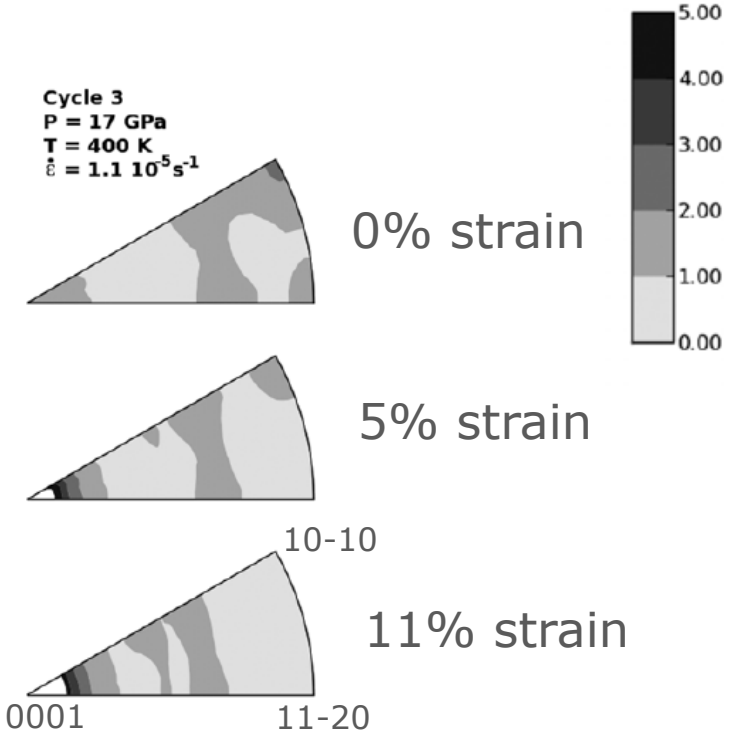

- Quantify preferred orientations
- With modeling: -> deformation mechanisms

Energy Dispersive configuration (NSLS, APS ID6)

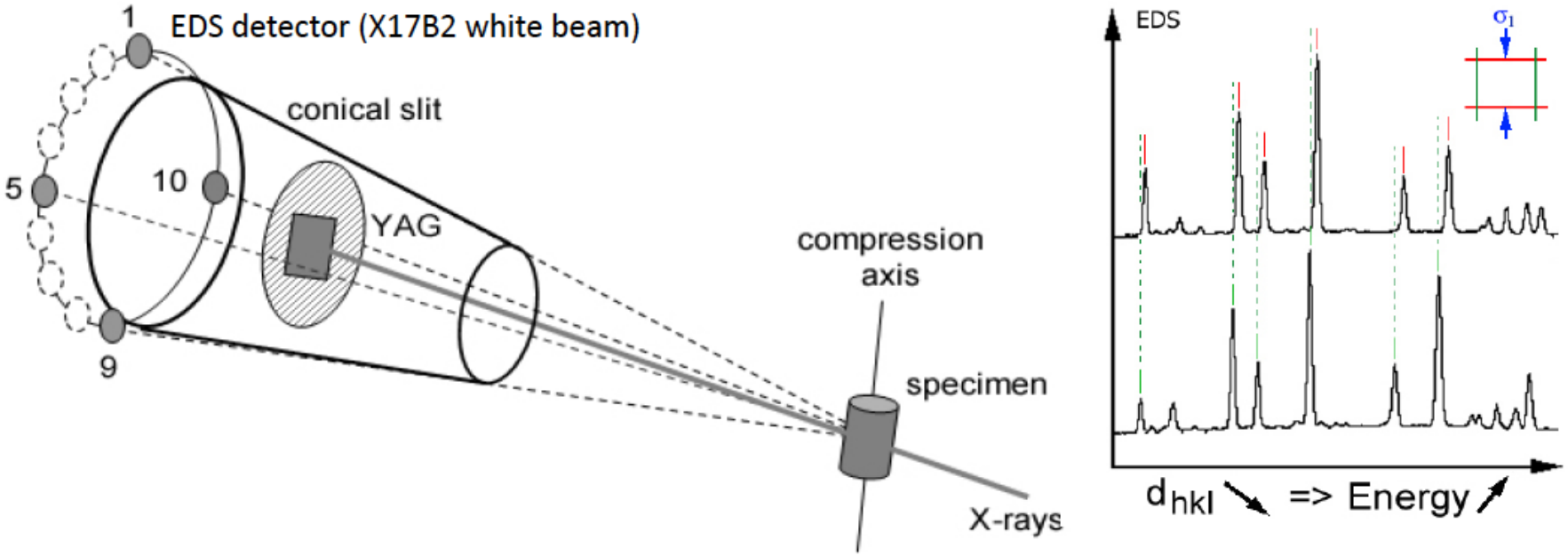

ⓘ Not desirable for preferred orientations and in case of strong grain recrystallisation and growth

Acoustic Emissions studies in the LVP / outlook for EBS

Earthquakes at depths

Those after ca. 50 km depth are not explained by friction theories.

… are these earthquakes induced somehow by mineralogical reactions ?

(and how do we test for this experimentally?)

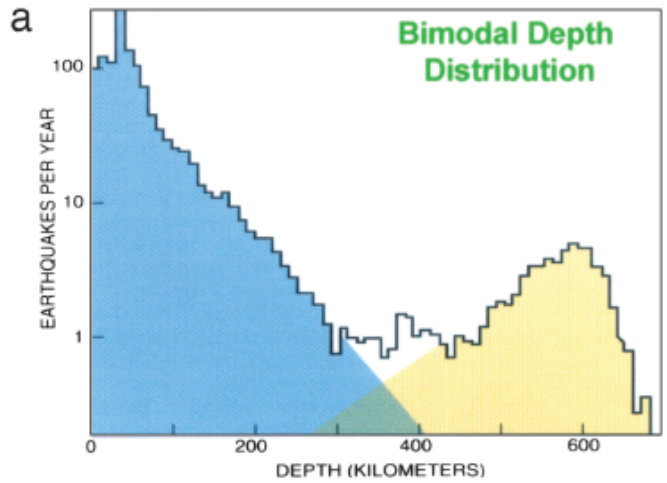

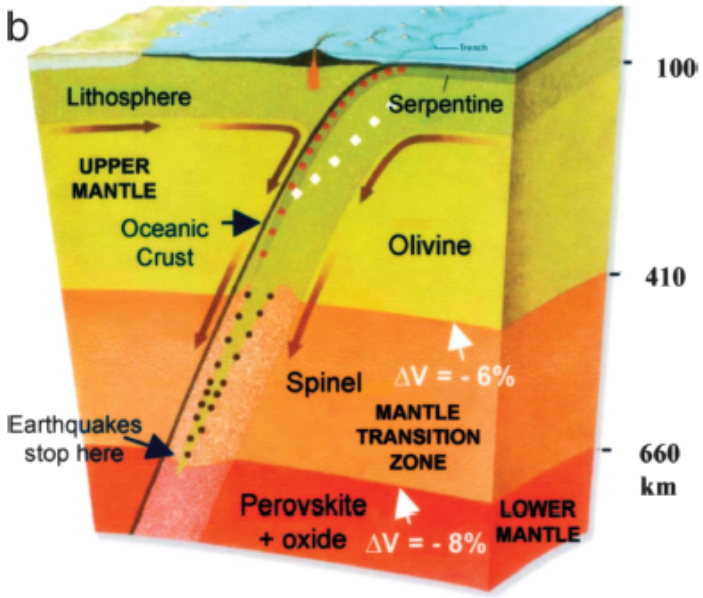

Green, 2007

Listening to rocks cracking under pressure:

LETTERS TO NATURE

as well as the temperature evolution calculated assuming two extreme cooling models (see Fig. 3 legend). The thermal histories of the lava lakes are closer to the conductive curve representing stagnant magma. Temperatures in Kilauea Iki depart from the ideal conduction model after $t^* \sim 0.0225$, which may be due to such observed processes as diapiric transfer of melt, crystal settling or gas exsolution[16]. However, there is no significant decrease of the interior temperature at early times, after the main degassing event ($t^* \approx 0.0045$; ref. 21 and M. Mangan, personal communication) or even after its complete cessation ($t^* \approx 0.013$). Comparison of the experimental (Fig. 3*a*) and the observed thermal (Fig. 3*b*) histories shows a remarkable similarity in terms of the temporal constancy of the interior temperature. This suggests the existence of a convective liquidus in the lava lake that is apparently near the actual magmatic liquidus itself. We suggest that it might not be the exsolution of gas that impedes convection[17], but the advancement of the growing crust which partitions from the magma the buoyancy necessary for convection.

In a closed system, although convection may be vigorous at the beginning of cooling and may be able to carry crystals into the interior and evacuate the large amount of latent heat released by the crystallization, its intensity soon diminishes. Kinetic effects are important in cooling magmas, as has been stressed in numerical modelling[22]. This is confirmed by recent observations[21,24] that crystallization of plagioclase in the Makaopuhi lava lake takes place at an undercooling of $<10^{-1}$ °C. The present experiments suggest that a thermal equilibrium will be achieved and the convective liquidus will be locked to the liquidus itself. They also show that, once the convective liquidus is reached, convective cooling may be negligible. This may also explain the results of studies[4,25] that show that the solidification

18. Helz, R. T. in *Magmatic Processes: Physico Principles* Spec. Publn 1 (ed. Mysen, B. O.) 241–258 (Geochemistry Society, 1987).
19. Helz, R. T. & Thornber, C. R. *Bull. volcanol.* **49**, 651–668 (1987).
20. Helz, R. T. *Geol. Soc. Am. Bull.* **101**, 578–594 (1989).
21. Mangan, M. T. & Helz, R. T. *Eos* **66**, 1133 (1985).
22. Brandeis, G., Jaupart, C. & Allègre, C. J. *J. geophys. Res.* **89**, 10161–10177 (1984).
23. Cashman, K. V. & Marsh, B. D. *Contr. Miner. Petrol.* **99**, 292–305 (1988).
24. Maaløe, S. *Am. J. Sci.* (submitted).
25. Peck, D. L., Hamilton, M. S. & Shaw, H. R. *Am. J. Sci.* **277**, 415–437 (1977).
26. Jaupart, C., Brandeis, G. & Allègre, C. J. *Nature* **308**, 535–538 (1984).
27. Turner, J. S., Huppert, H. E. & Sparks, R. S. J. *J. Petrol.* **27**, 397–437 (1986).
28. Huppert, H. E. & Sparks, R. S. J. *Contr. Miner. Petrol.* **75**, 279–289 (1980).
29. Carslaw, H. S. & Jaeger, J. C. *Conduction of Heat in Solids* (Clarendon Press, Oxford, 1959).

ACKNOWLEDGEMENTS. We thank Mark Smith and George Bergantz for discussions, Rosalind Helz and Margaret Mangan for discussions on the Hawaiian lava lakes, and Alexander McBirney and Steve Tait for their reviews. This work is supported by the NSF, NASA and IPGP (France).

Acoustic emissions and shear instabilities during phase transformations in Si and Ge at ultrahigh pressures

Charles Meade & Raymond Jeanloz

Department of Geology and Geophysics, University of California, Berkeley, California 94720, USA

ACOUSTIC emissions are commonly observed at low pressures as they are characteristic of brittle deformation[1,2]. Most solids are ductile above a few gigapascals (GPa), and acoustic emissions have not been recorded from solids above 5 GPa. Here we describe

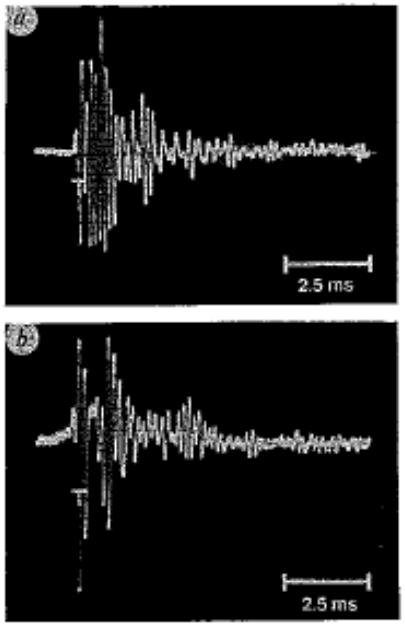

FIG. 1 Oscilloscope traces of the acoustic emissions from diamond-cell samples. The emissions were recorded with an acoustic microphone placed near the diamond cell. The Si emissions (*a*) were detected on compression at peak pressures of 20 GPa. The emissions from Ge (*b*) were recorded on decompression at peak pressures of 70 GPa.

acoustic emissions: sudden release of elastic energy
taken as proxy for ««brittle-like»» events in the samples

Deformation-DIA (HP-HT)
X
Synchrotron x-rays
X
acoustic emission (AE) recording

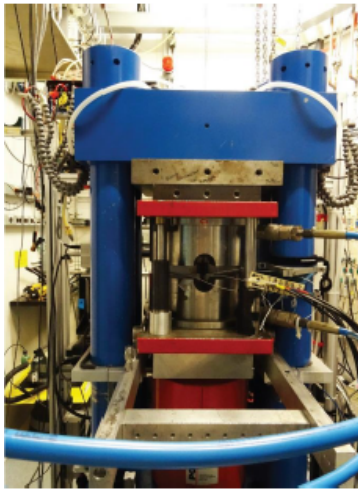

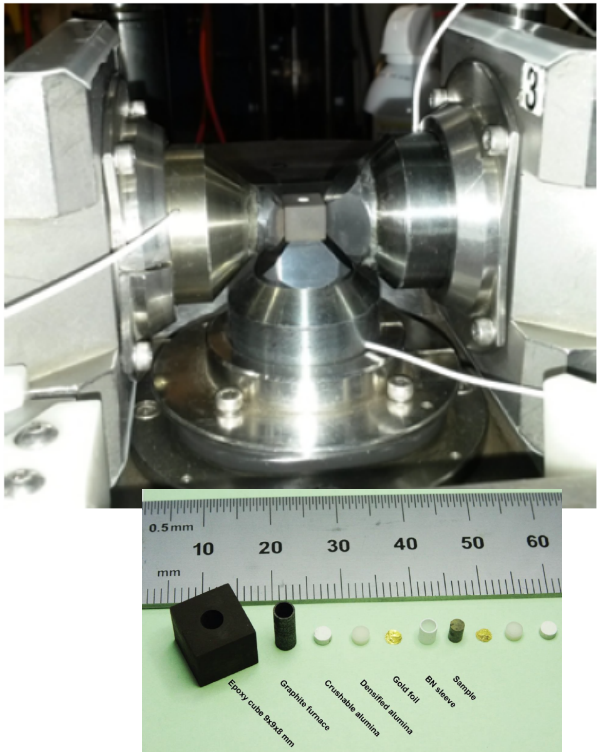

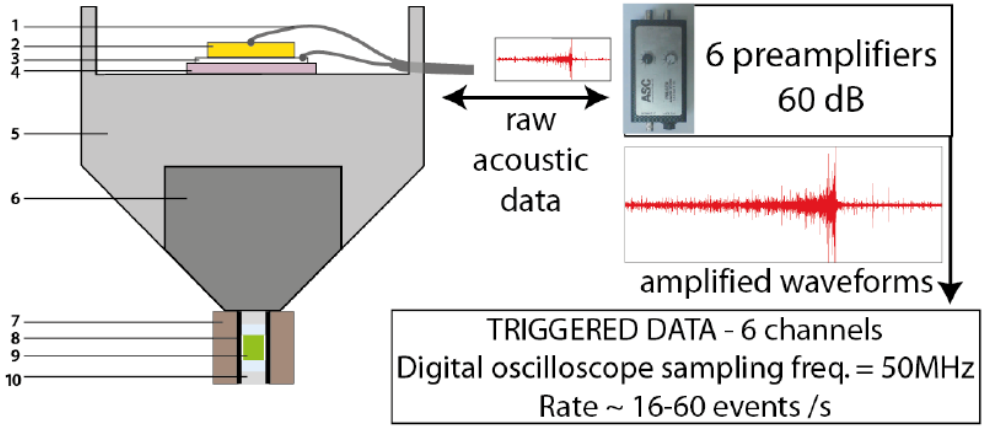

Gasc et al, 2011

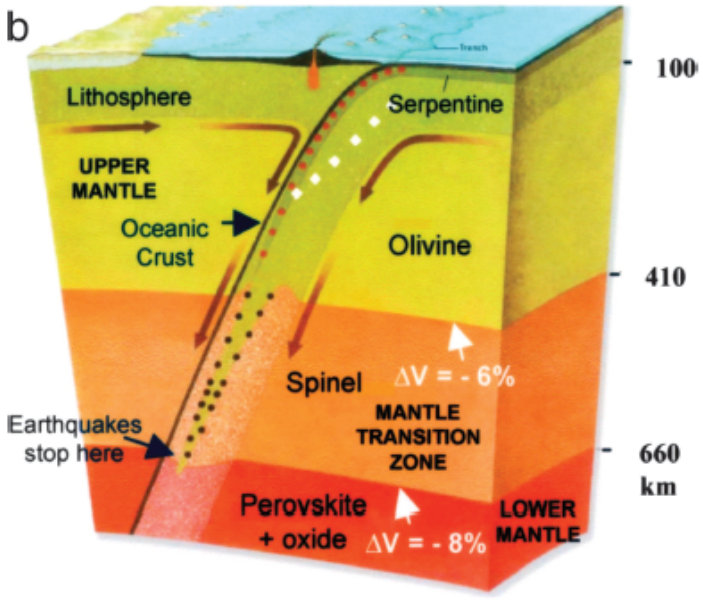
b
Lithosphere
Serpentine
UPPER
MANTLE
Oceanic
Crust
Olivine
Spinel
ΔV = - 6%
MANTLE
TRANSITION
ZONE
Earthquakes
stop here
Perovskite
+ oxide
ΔV = - 8%
LOWER
MANTLE
100
410
660
km

Green, 2007

$(Mg,Fe)_2SiO_4$ olivine requires too high pressures
-> use an iso-structural system (« analog »)

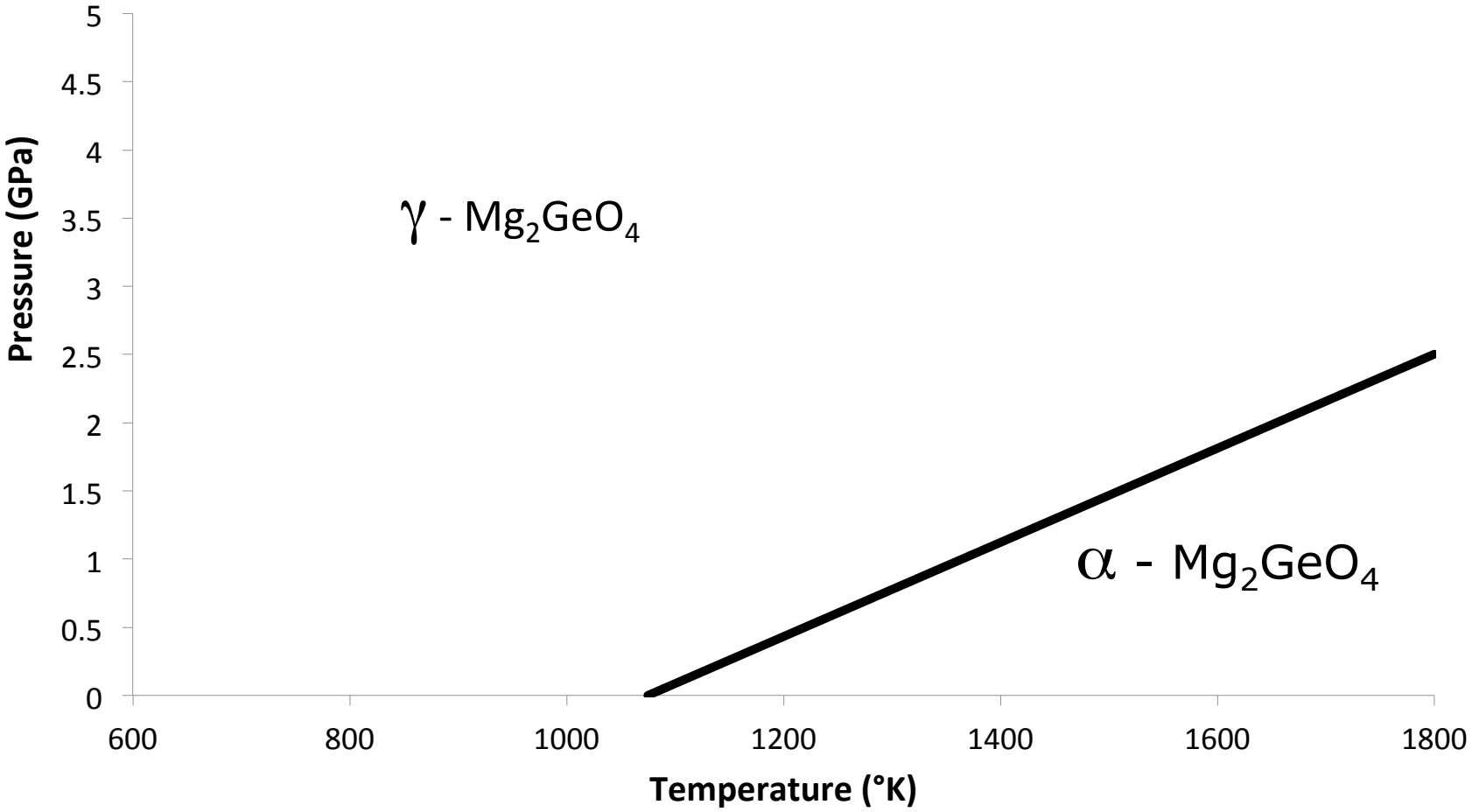

Modified from Burnley and Green, 1991

Back in the 1990…
Can we extend this to the mantle ?

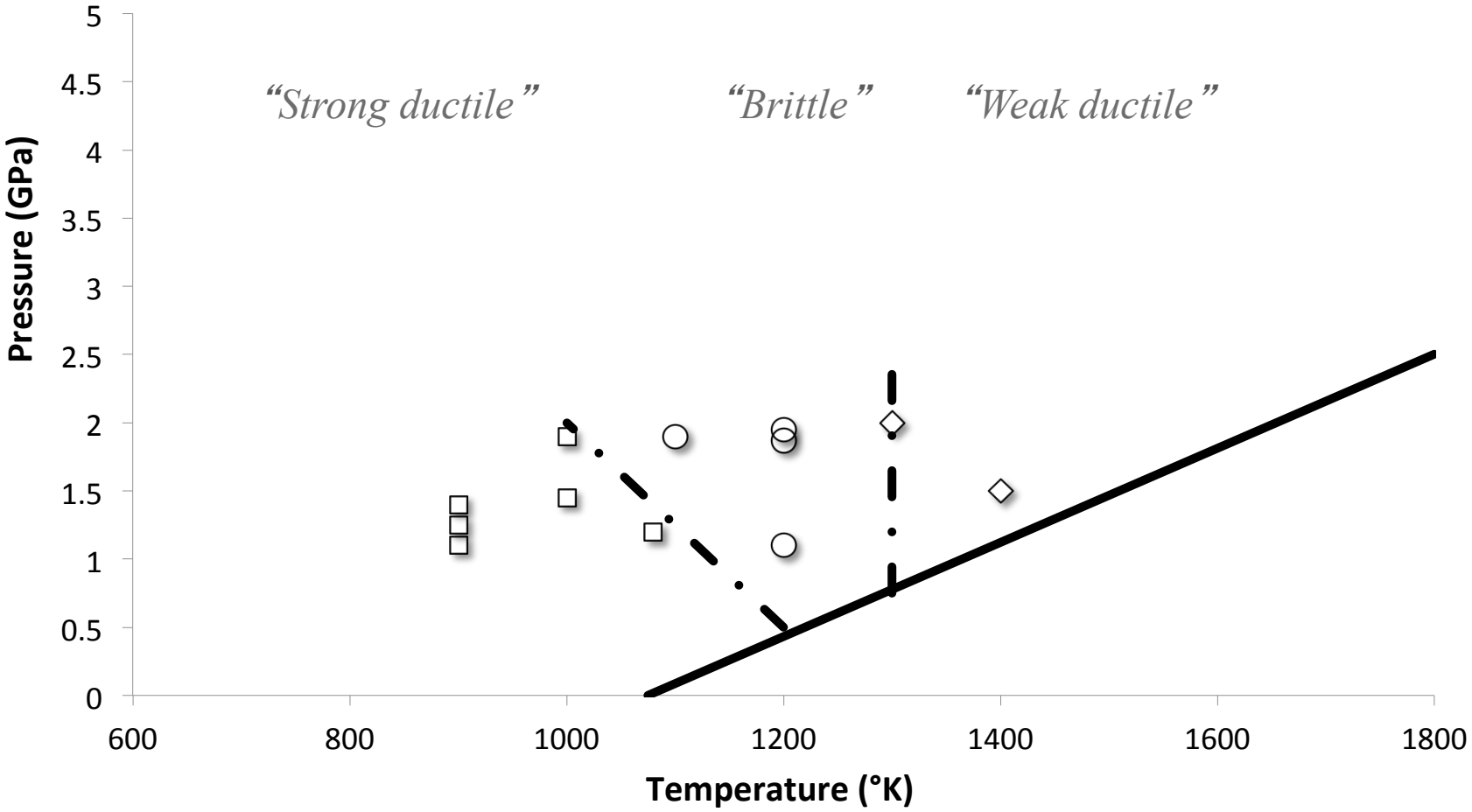

Mechanical Boundaries from Burnley and Green, 1991,

based on microstructures

Extending to higher pressures, adding AE monitoring and recording σ in real-time.

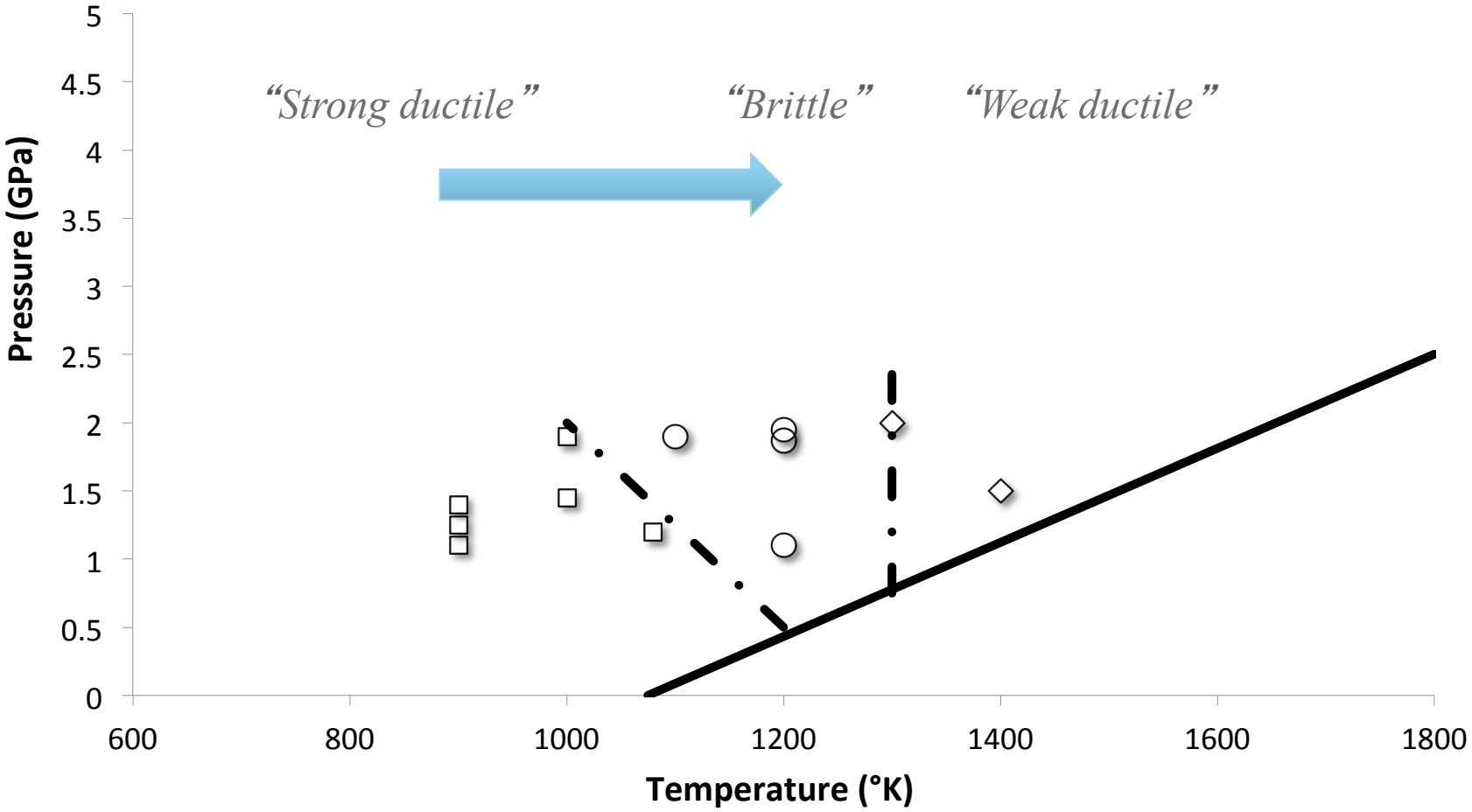

Mechanical Boundaries from Burnley and Green, 1991,

based on microstructures

Olivine to spinel transition in Mg_2GeO_4 system

Pre-sintered Ge-olivine, average grain size 30 microns, courtesy H.W. II Green
Effective mean stress (pressure) = 4 GPa(0.25)

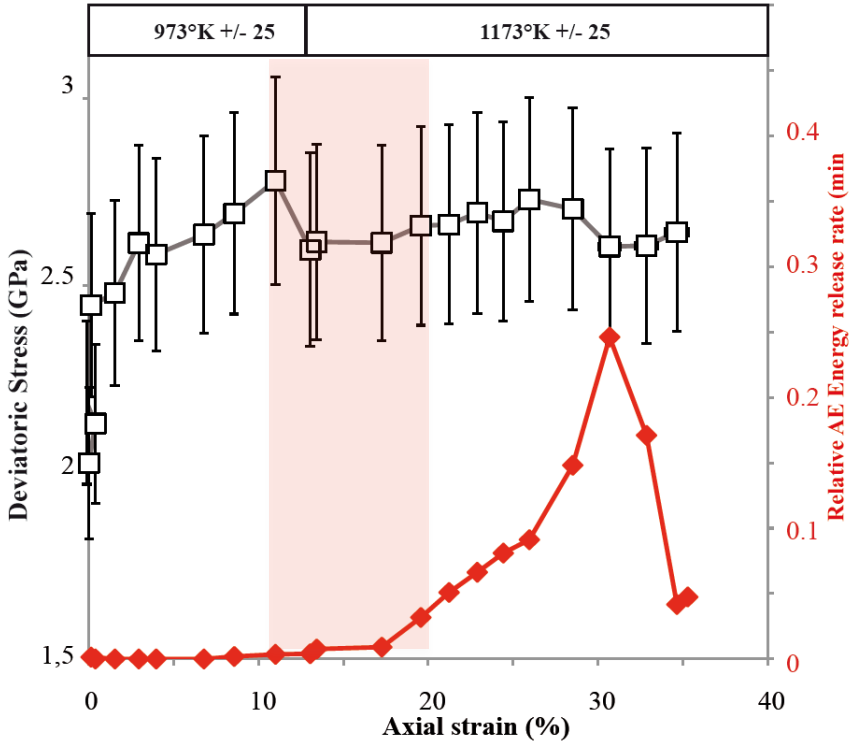

Schubnel et al, 2013

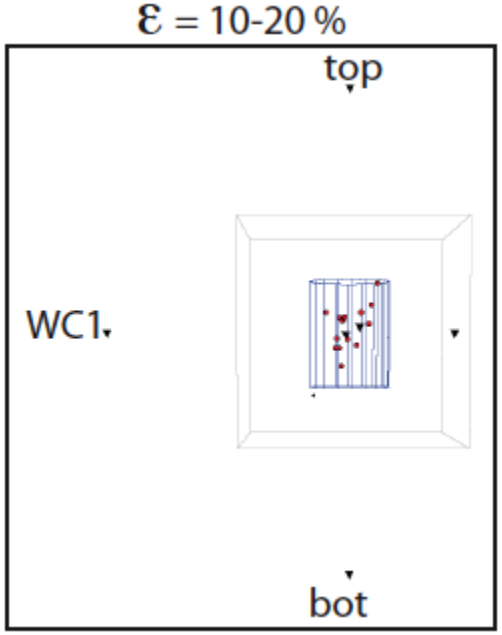

Olivine to spinel transition in Mg_2GeO_4 system

Pre-sintered Ge-olivine, average grain size 30 microns, courtesy H.W. II Green
Effective mean stress (pressure) = 4 GPa(0.25)

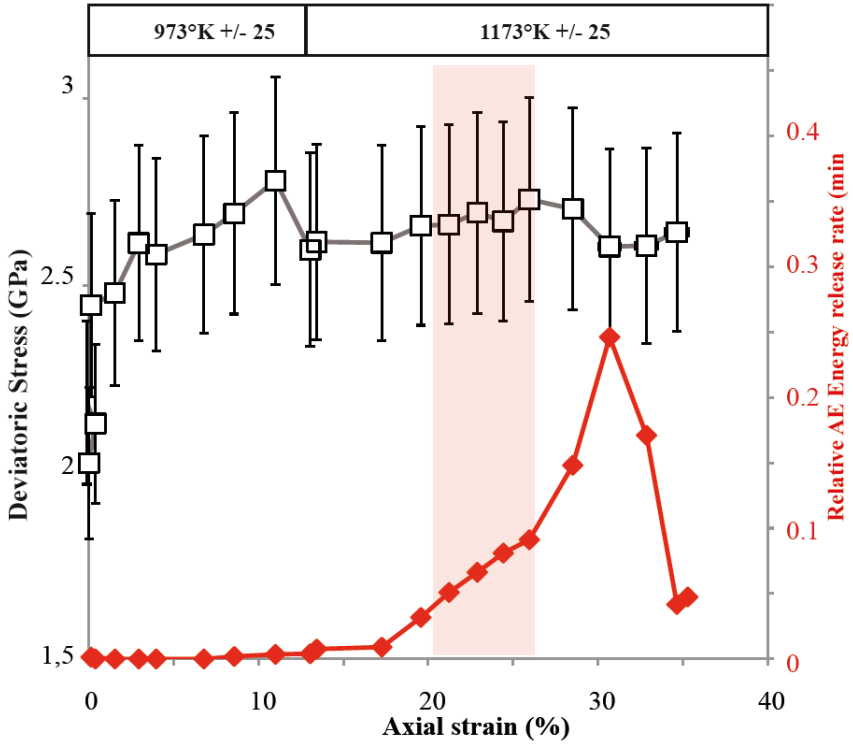

Schubnel et al, 2013

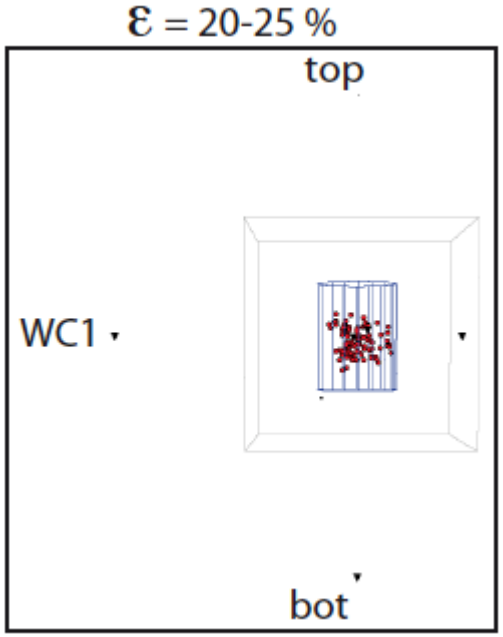

Olivine to spinel transition in Mg_2GeO_4 system

Pre-sintered Ge-olivine, average grain size 30 microns, courtesy H.W. II Green
Effective mean stress (pressure) = 4 GPa(0.25)

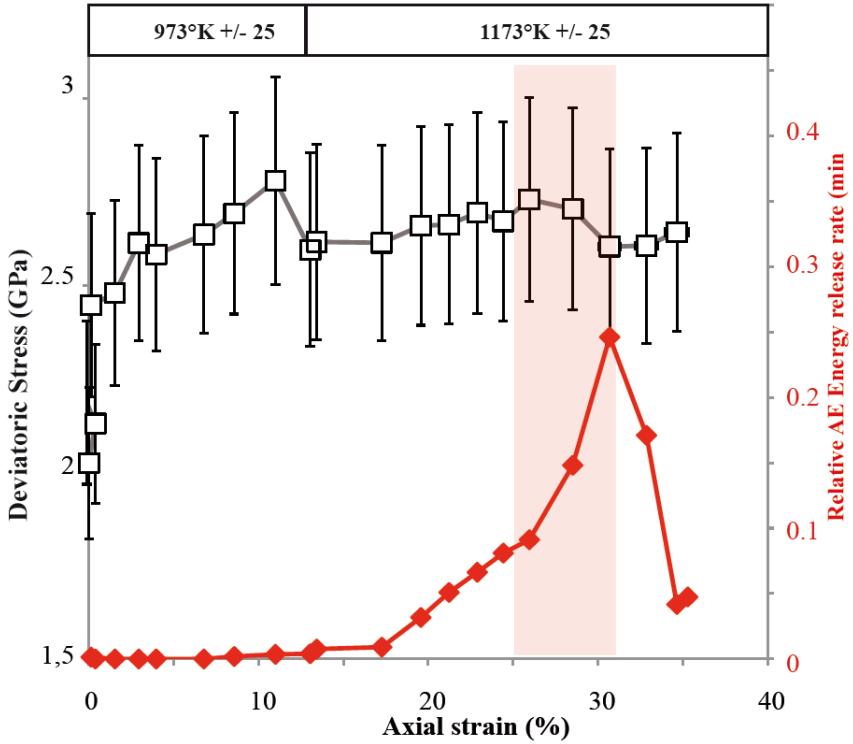

Schubnel et al, 2013

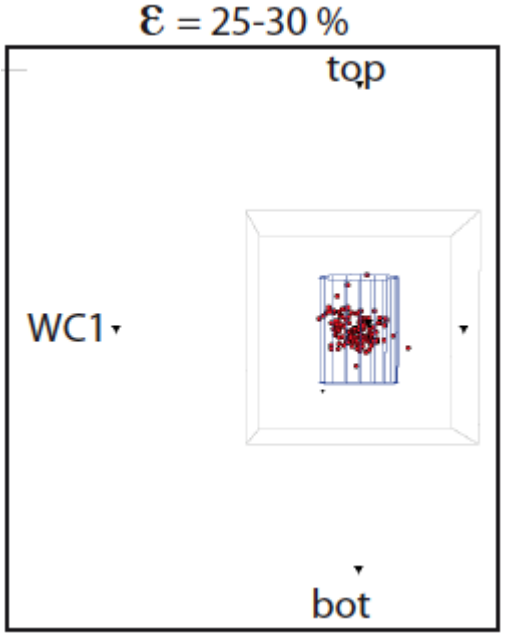

Olivine to spinel transition in Mg_2GeO_4 system

Pre-sintered Ge-olivine, average grain size 30 microns, courtesy H.W. II Green
Effective mean stress (pressure) = 4 GPa(0.25)

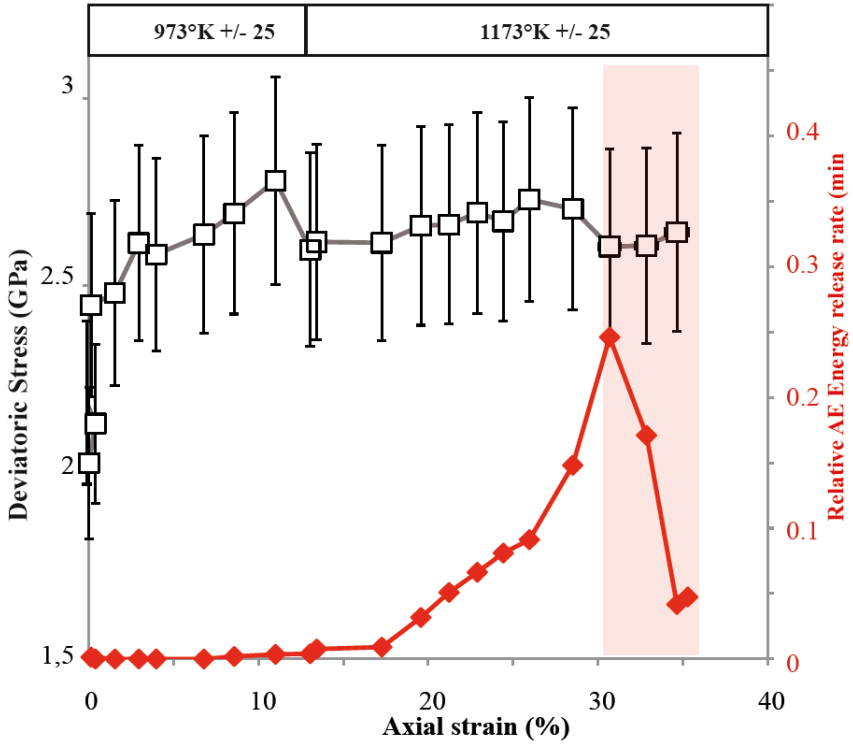

Schubnel et al, 2013

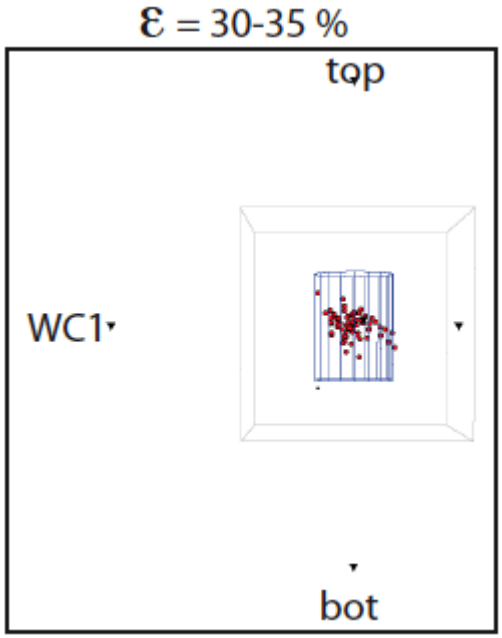

Sources characteristics

Moment Tensor inversion for 42 largest AE events (unclipped):

❑ 90 % Shear, i.e. less than 10% volumetric component

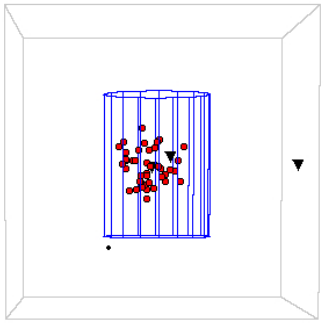

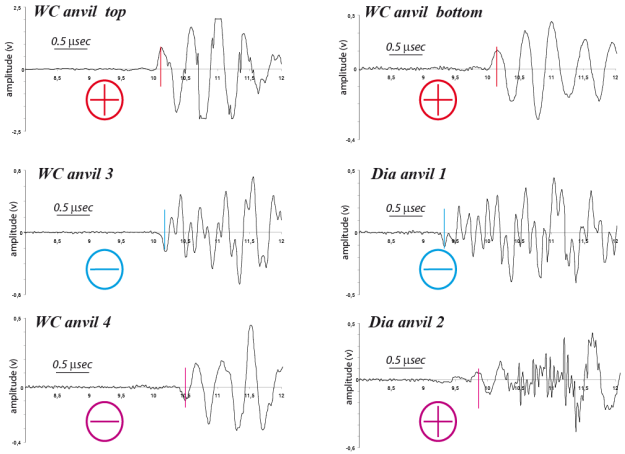

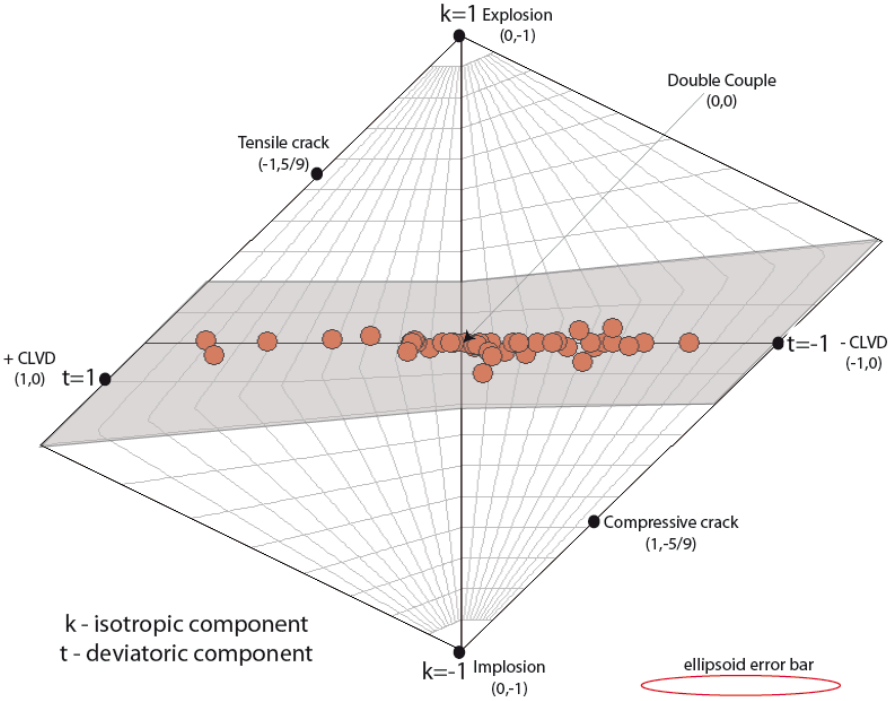

Schubnel et al, 2013

AE statistics (continuous recording)

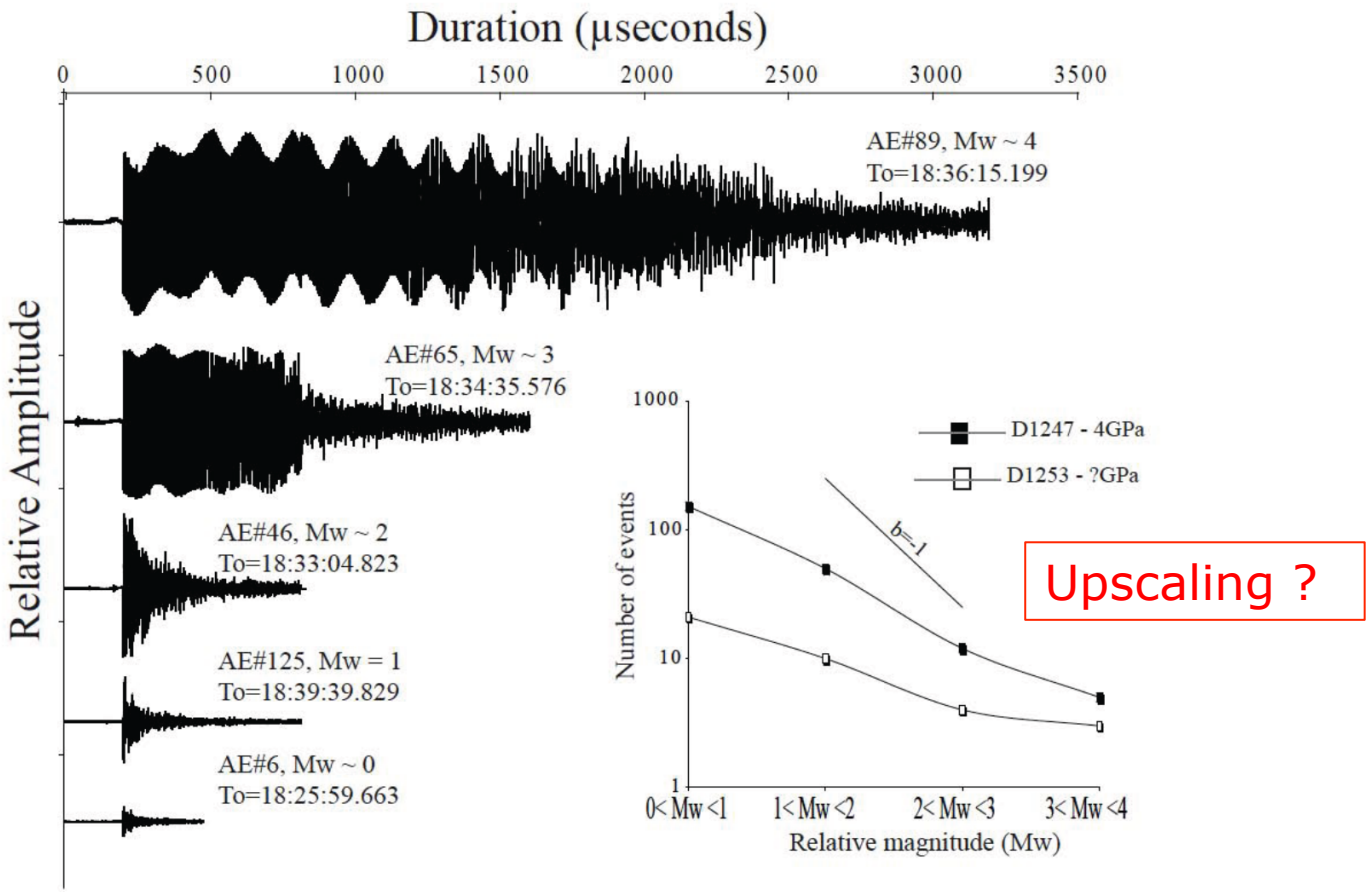

Upscaling ?

Schubnel et al, 2013

Mineralogical reactions in the downgoing slab and intermediate depth seismicity…

- Several rocks types investigated…
- Incel et al, 2017: AE are not specifically associated with a major fluid release (ie. lws breakdown).
- Ferrand et al, 2017: AE in dehydrating serpentinites occur for specific compositions and are due to a stress transfer at grain scales.